

Dear Executive Editor SE,

we are deeply grateful for the critical comments that helped us to improve the clarity and quality of the manuscript. In this new version we have revised the English writing, shortened and reorganised the text in order to avoid repetitions and too generic statements. We accepted all the corrections listed in your comment.

In particular, we defined the magmatic pressure as either excess pressure (ΔP_e , magmatic minus lithostatic pressure but below the tensile strength of wall rocks) or over pressure (or driving pressure ΔP_o , which is the magmatic pressure exceeding tensile strength of wall rocks) according to Gudmundsson (2012). The first pertains to the FEMs using isolated magma chambers (single or double), while the second is used for models with connected magma chambers (with conduit/feeding system).

Please find attached here the manuscript with the tracked changes, along with a clean version. We hope this presentation can fulfil your requests.

With our best regards,

On the behalf of Authors

Silvia Massaro

Analysing stress field conditions of the Colima Volcanic Complex (Mexico) by integrating FEM simulations and geological data

Silvia Massaro^{1,2}, Roberto Sulpizio^{1,2,3}, Gianluca Norini², Gianluca Groppelli², Antonio Costa¹, Lucia Capra⁴, Giacomo Lo Zupone⁵, Michele Porfido⁶, Andrea Gabrieli⁷

¹Istituto Nazionale di Geofisica e Vulcanologia, Via D. Creti 12, 40128, Bologna, Italy.

²Istituto di Geologia Ambientale e Geoingegneria, Consiglio Nazionale delle Ricerche, Via M. Bianco 9, 20131, Milan, Italy.

³Dipartimento di Scienze della Terra e Geoambientali, Via E. Orabona 4, 70125, Bari, Italy.

⁴Centro de Geociencias, Universidad Nacional Autonoma de Mexico, Queretaro, Mexico.

⁵Institute of New Energy and Low-carbon Technology, Sichuan University, Chengdu, PRC.

⁶Alumni Mathematica, Dipartimento di Matematica, Via E. Orabona 4, 70125, Bari, Italy.

⁷Hawai'i Institute of Geophysics and Planetology, 1680 E-W Road, Honolulu, Hawai'i 96922, USA.

*corresponding author: Silvia Massaro (silvia.massaro@ingv.it)

Abstract

In the last decades **Finite Element Modelling** have become very popular tools in volcanological studies, **increasing the relevant parameters considered in their calculations, and raising complex geometry with introduction** of multiple reservoirs, topography, and heterogeneous distribution of host rock mechanical properties. **In spite of this**, the influence of geological **information** on the numerical simulations is still poorly considered. In this work a 2D Finite Element Modelling of **Colima Volcanic Complex (Mexico)** is provided by using the LInear Static Analysis (LISA) software, in order to investigate the stress field conditions at increasing **detail of geological data**. By integrating the published geophysical, volcanological and petrological data, we **modelled the stress field** considering either one or two magma chambers connected to the surface via dykes or isolated (not connected) in the elastic host rocks (**considered homogeneous and not homogeneous**). We also **introduced tectonic disturbance, considering the effects of direct faults bordering the Colima Rift and imposing an extensional far field stress of 5 MPa. We run the model using gravity in the calculations.** Our results suggest that an appropriate set of geological data is of pivotal importance for **obtaining reliable numerical outputs, which can be considered as proxy for natural systems. Beside and beyond the importance of geological data in FEM simulations, the model runs using the complex feeding system geometry and tectonics show how the present-day Colima volcanic system can be considered in equilibrium by stress state point of view, in agreement with the long lasting open conduit dynamics that lasts since 1913.**

1 Introduction

Utente di Microsoft Office 22/9/20 11:10
Formattato: Italiano

Utente di Microsoft Office 22/9/20 11:10
Formattato ... [1]

Utente di Microsoft Office 22/9/20 11:30
Formattato ... [2]

Utente di Microsoft Office 22/9/20 11:10
Formattato ... [3]

Utente di Microsoft Office 22/9/20 11:10
Formattato ... [4]

Utente di Microsoft Office 22/9/20 11:10
Formattato ... [5]

Utente di Microsoft Office 22/9/20 11:41
Eliminato: numerical methods

Utente di Microsoft Office 22/9/20 15:36
Formattato: Giustificato, Nessuna, Spazio Dopo: 12 pt, Nessun controllo righe isolate

Silvia 16/9/20 17:49
Eliminato: since capable of considering

Utente di Microsoft Office 22/9/20 11:30
Eliminato: taking into account...ncre ... [6]

Silvia 16/9/20 20:42
Eliminato: presence

Utente di Microsoft Office 22/9/20 11:42
Eliminato: Although the widespread availability of geodetic data is keep growing

Silvia 16/9/20 20:43
Eliminato: data ...nformation on the ... [7]

Utente di Microsoft Office 22/9/20 11:47
Eliminato: occurring around the Colima Volcanic Complex (CVC, Mexico)

Silvia 16/9/20 20:43
Eliminato: the details of

Utente di Microsoft Office 22/9/20 11:47
Eliminato: ed

Silvia 16/9/20 20:55
Eliminato: and geophysical input ... [8]

Utente di Microsoft Office 22/9/20 11:50
Eliminato: provide ...odelled the stre ... [9]

Silvia 28/9/20 09:51
Eliminato: graben

Utente di Microsoft Office 22/9/20 11:52
Eliminato: . We test the methodology by using athrough a gravitational modelling with by using different geometrical configurations and constraints (i.e. magma chamber dimensions, depth, overpressure), constraints (i.e., magma chamber dimensions and depth, dyke extension, magmatic overpressure, extensive far-field stress)...e run the ... [10]

Silvia 28/9/20 09:52
Eliminato: of

Utente di Microsoft Office 22/9/20 11:58
Eliminato: the ...atural systems. Be ... [11]

101

102 Magmatism and tectonism are strongly related to the regional and local stress fields, affecting both

103 the orientation of faults and the location of volcanic vents (Geyer et al., 2016). The stress field around

104 a magmatic source originates from three main contributions: (1) the background stress, composed of

105 a vertical gravitational load, a lateral horizontal load (lithostatic confinement), and tectonic regime;

106 (2) the stress field caused by the loading of the volcano edifice; and, (3) the stress field generated by

107 the magmatic pressure (e.g. Martí and Geyer, 2009; Currenti and Williams et al., 2014). In recent

108 years, a large number of semi-analytical and numerical methods have been proposed for the solution

109 of stress field state of natural systems (e.g. Cayol and Cornet, 1998; Simms and Garven, 2004;

110 Manconi et al., 2007; Long and Grosfils, 2009; Currenti et al., 2010; Currenti and Williams et al.,

111 2014; Zehner et al., 2015), taking into account the static elastic deformation in a multi-layered half-

112 space (e.g. Dieterich and Decker, 1975; Bonafede et al., 2002; Wang et al., 2003; Gudmundsson and

113 Brenner, 2004; Zhao et al., 2004; Pritchard and Simons, 2004; Gottsmann et al., 2006; Geyer and

114 Gottsmann, 2010; Zhong et al., 2019). Following the successful application in mechanical

115 engineering, fluid dynamics and thermodynamics (e.g., Gutiérrez and Parada, 2010; Gelman et al.,

116 2013), the use of Finite Element Method (FEM) has been extensively introduced in volcanology, in

117 order to investigate the effects of topography, lithologic heterogeneities, tectonic stresses and the

118 gravity field on stress state of volcanic systems (e.g. Fujita et al., 2013; Carcho and Gálan del Sastre,

119 2014; Bunney, 2014; Ronchin et al., 2015; Hickey et al., 2015; Cabaniss et al., 2019; Rivalta et al.,

120 2019).

121 The use of FEM for volcanic systems has several examples, which span from the influence of layered

122 materials on the surface deformation process during volcanic inflation (e.g. Darwin volcano,

123 Galapagos Islands; Manconi et al., 2007; Albino et al., 2010) to processes affecting chamber rupture

124 (e.g. Grosfils, 2007; Long and Grosfils, 2009).

125 The local stress around a volcanic feeding system depends on the geometry of the magma plumbing

126 system, including chamber(s) and dykes forming it, and on the mechanical properties of the host rock

127 around it (e.g. Martí and Geyer, 2009), and especially on changes in Young Modulus (e.g.

128 Gudmundsson et al., 2011; Jeanne et al., 2017; Heap et al., 2020). For instance, limestones, lava

129 flows, welded pyroclastic deposits and subvolcanic rocks can be very stiff (high Young Modulus; ca.

Utente di Microsoft Office 22/9/20 12:07
Eliminato: represent in volcanic active areas essential aspects when interpreting volcanic unrest and forecasting volcanic eruptions since they

Utente di Microsoft Office 22/9/20 16:08
Formattato: Spazio Dopo: 0 pt, Tabulazioni: 2,75 cm, Left

Silvia 16/9/20 21:06
Eliminato: , two fundamental aspects when interpreting volcanic unrest and forecasting volcanic eruptions ...Geyer et al., 201... [12]

Utente di Microsoft Office 22/9/20 12:09
Eliminato: corresponding to... ..it... [13]

Silvia 16/9/20 21:17
Eliminato: geological and volcanological

Utente di Microsoft Office 22/9/20 16:00
Eliminato: have been proposed ...e... [14]

Antonio Costa 27/9/20 12:05
Eliminato: in ...or volcanic areas ... [15]

Silvia 16/9/20 21:18
Eliminato: which vary

Utente di Microsoft Office 22/9/20 16:09
Eliminato: varying...hich span ...r... [16]

Silvia 16/9/20 21:20
Eliminato: strongly ...depends on the... [17]

Utente di Microsoft Office 22/9/20 16:10
Eliminato: layered ...ost rock around... [18]

Silvia 16/9/20 21:22
Eliminato: m

Utente di Microsoft Office 22/9/20 16:17
Eliminato: units ...eposits and intru... [19]

Silvia 16/9/20 21:23
Eliminato: m...dulus; from ... [20]

1.7-27 GPa for limestones, Touloukian, 1981; ca. 5.4 GPa for volcanic rocks, Heap et al., 2020), but young and non-welded pyroclastic units may be very soft (low Young Modulus; ca. 1.7 – 3.1 GPa, Margottini et al., 2013). Therefore, the local stress may abruptly change from one layer to another (e.g., Gudmundsson, 2006). Irrespective of the scope of the numerical investigation, the importance of applying accurate physical constraints to FEM modelling was already discussed in many studies (e.g., Folch et al., 2000; Newman et al., 2001; Fernandez et al., 2001; Currenti et al., 2010; Geshi et al., 2012). However, in the last decade few investigations have been carried out to assess the influence of the amount and quality of geological data into FEM computations (Kinvig et al., 2009; Norini et al., 2010, 2019; Cianetti et al., 2012; Ronchin et al., 2013; Chaput et al., 2014). To bridge this gap, in this work we use the Linear Static Analysis (LISA) software (version 8.0; www.lisafea.com) to study the subsurface stress field state at Colima Volcanic Complex (CVC, Mexico) at increasing geological detail.

The CVC area is a good candidate for testing the response of FEM software against different geological conditions, being constituted by a large volcanic complex (Lungarini et al., 2005) within a tectonic graben filled with volcanoclastic material (Fig. 1a; Norini et al., 2010, 2019). The FEM was run starting from simple homogeneous vs. stratified lithology of subsurface, and successively detailed by the addition of single and double magma chamber, feeder dykes, faults, and extensional far field tectonic stress (Fig. 1b).

2 The Colima Volcanic Complex (Mexico)

2.1 Geological framework

The Pleistocene-Holocene CVC is one of the most prominent volcanic edifices within the Trans-Mexican Volcanic Belt (TMVB) (Macías et al., 2006; Capra et al., 2016; Norini et al., 2019; Fig. 1a). In this area, the Rivera microplate and the Cocos plate subduct beneath the North America plate along the Middle American Trench, (Stock and Lee, 1994), forming a triple junction that delimits the tectonic units known as the Jalisco Block (JB) and the Michoacán Block (MB) (Luhr et al., 1985;

Silvia 16/9/20 21:23

Eliminato: to

Silvia 16/9/20 21:23

Eliminato: whereas

Utente di Microsoft Office 22/9/20 16:18

Eliminato: g's

Silvia 16/9/20 21:23

Eliminato: m

Silvia 16/9/20 21:23

Eliminato: Consequently

Silvia 16/9/20 21:23

Eliminato: change

Antonio Costa 27/9/20 12:08

Eliminato: rheological

Silvia 16/9/20 21:29

Eliminato: This implies that geology of the volcanic area needs to be considered as more accurate as possible.

Silvia 16/9/20 21:33

Eliminato: behaviour

Silvia 16/9/20 21:33

Eliminato: in an elastic domain

Utente di Microsoft Office 22/9/20 16:21

Eliminato: when

Utente di Microsoft Office 22/9/20 16:21

Eliminato: improving the description of

Utente di Microsoft Office 22/9/20 16:21

Eliminato: constraints

Silvia 16/9/20 18:00

Eliminato: to

Silvia 16/9/20 17:54

Eliminato: significant topographic load;

Silvia 16/9/20 18:20

Eliminato: ,

Utente di Microsoft Office 22/9/20 16:22

Eliminato: covered by

Utente di Microsoft Office 22/9/20 16:29

Eliminato: In this study, geophysical and petrological data (e.g. Spica et al., 2017; Massaro et al. 2018, 2019)we assess how and at what extent, the addition of geological, volcanological, petrological data along with geophysical observations (e.g. Spica et al., 2017; Massaro et al. 2018, 2019) as model constraints (i.e. stratigraphy, geometry of the plumbing system, magmatic overpressure, extensive tectonic regime, local fault systems) may affect the outputs (Fig. 1b), also providing a large-scale picture of stress distribution in the CVC subsurface. .

Silvia 19/9/20 17:36

Eliminato: producing great deformation and fragmentation of the continental plate

Silvia 19/9/20 17:36

Eliminato: and

256 Allan, 1986; Rosas-Elguera et al., 1996; Rosas-Elguera et al., 1997; Ferrari and Rosas- Elguera,
 257 1999; Rosas-Elguera et al., 2003; Frey et al., 2007). The three rifts of this system are the Tepic-
 258 Zacoalco (TZR), the Chapala-Tula (CTR), and the Colima Rift (CR). The still active NS trending CR
 259 was formed during a rifting phase occurred after the Late Cretaceous–Paleogene compressive and
 260 transpressive phase (Allan, 1986; Serpa et al., 1992; Bandy et al., 1995; Cortés et al., 2010). While
 261 opening, CR was gradually filled with Pliocene–Quaternary lacustrine sediments, alluvium and
 262 colluvium (e.g. Allan, 1986; Allan et al., 1991; Norini et al., 2010). The geometry, kinematics and
 263 dynamics of the CR have been studied on the basis of field, seismic, and geodetic data, mainly
 264 collected in its northern and central sectors (see Fig. 1 in Norini et al., 2010).

265 The magnitude of vertical displacement of the northern and central sectors is ca. 2.5 km by adding
 266 the topographic relief of the bounding fault scarps (1.5–1.6 km) to the calculated sediment depth
 267 (Allan, 1985; Serpa et al., 1992). Field data and focal mechanism solutions are consistent with a
 268 direction of opening of the northern and central sectors oriented from E-W to NW-SE, with a mainly
 269 normal and minor right-lateral displacements of the bounding faults (Barrier et al., 1990; Suárez et al.,
 270 1994; Rosas-Elguera et al., 1996; Garduño-Monroy et al., 1998; Norini et al., 2010, 2019). In contrast
 271 to field and seismic evidence of long-term slightly dextral oblique extension, recent GPS geodetic
 272 measurements suggest a possible left oblique extension of the CR (Selvans et al., 2011). In both cases,
 273 the stress regime is extensional with an E-W orientation of the minimum horizontal stress in the CVC
 274 basement (Barrier et al., 1990; Suárez et al., 1994; Rosas-Elguera et al., 1996; Selvans et al., 2011;
 275 Norini et al., 2010, 2019).

276 The CVC stands within the central sector of the CR, on top of the Cretaceous limestones, Late
 277 Miocene-Pleistocene volcanic rocks, and Pliocene-Holocene lacustrine sediments, alluvium, and
 278 colluvium (Allan, 1985, 1986, 1991; Cortès, 2005; Norini et al., 2010; Escudero and Bandy, 2017). It
 279 is formed by three andesitic stratovolcanoes; Cantaro (2900 m a.s.l.), Nevado de Colima (4255 m
 280 a.s.l.) and, in the southern part, the youngest and active Volcàn de Colima (3763 m a.s.l.) (Norini et
 281 al., 2019 and reference therein; Fig. 1a).

282 2.2 Eruptive activity

284 The eruptive history of the CVC started in the northeast area with the formation of Cantaro volcano

- Silvia 19/9/20 17:54
Eliminato: where the CVC is emplaced (Allan, 1986; Escudero and Bandy, 2017).
- Antonio Costa 27/9/20 12:10
Eliminato: Colima Rift (
 Antonio Costa 27/9/20 12:10
Eliminato:)
- Silvia 19/9/20 18:07
Eliminato: n
- Silvia 19/9/20 17:36
Eliminato: extensional
- Silvia 19/9/20 18:07
Eliminato: . The rifting phase deformed Cretaceous marine limestones, Jurassic–Tertiary metamorphosed clastic and volcaniclastic sediments, Cretaceous–Tertiary intrusive rocks and Tertiary-Quaternary volcanic deposits along sub-vertical crustal faults
- Silvia 16/9/20 19:00
Eliminato: amount
- Silvia 19/9/20 17:48
Eliminato: estimated to be at least
- Utente di Microsoft Office 22/9/20 16:32
Eliminato: sinistral
- Silvia 19/9/20 18:03
Eliminato: mainly extensional
- Utente di Microsoft Office 22/9/20 16:30
Eliminato: ve
- Silvia 19/9/20 18:03
Eliminato: ,
- Silvia 19/9/20 17:49
Eliminato: an approximately
- Silvia 19/9/20 17:49
Eliminato: of the CVC
- Silvia 19/9/20 17:55
Eliminato: The volcanic complex is affected and displaced by the N-S/NNE-SSW-trending recent-active crustal faults of the CR, controlling the geometry and location of the volcano feeding system (Fig. 1a). Indeed, the CVC was
- Silvia 19/9/20 17:58
Eliminato: aligned parallel to the CR bounding faults
- Utente di Microsoft Office 22/9/20 16:41
Eliminato: the northern inactive
- Silvia 19/9/20 18:03
Eliminato: volcano
- Utente di Microsoft Office 22/9/20 16:41
Eliminato: following by the inactive
- Utente di Microsoft Office 22/9/20 16:42
Eliminato:), which are all displaced by the N-S/NNE-SSW-trending recent-active crustal faults of the CR
- Utente di Microsoft Office 22/9/20 16:42
Eliminato: (

321 at ca. 1-1.5 Ma followed by Nevado de Colima at ca. 0.53 Ma, which is composed of voluminous
 322 andesitic lava domes and deposits associated with caldera forming eruptions and partial sector
 323 collapses (Robin et al., 1987; Roverato et al., 2011; Roverato and Capra, 2013; Cortès et al., 2019).
 324 The youngest Volcàn de Colima comprises the Paleofuego edifice, which suffered several sector
 325 collapses that formed a horseshoe-shaped depression where the new active (also known as Volcàn de
 326 Fuego) cone grew up. Its activity was characterised by dome growths and collapses, extrusion of lava
 327 flows, Vulcanian and occasionally sub-Plinian explosive eruptions (Saucedo et al., 2010; Massaro et
 328 al., 2018, 2019).

Silvia 19/9/20 18:04
 Eliminato: . The volcanic activity of ... [21]

Utente di Microsoft Office 22/9/20 16:44
 Eliminato: , now considered one of the most active volcanoes of the world, ... [22]

Silvia 19/9/20 18:08
 Eliminato: (also known Volcàn de F... [23]

Utente di Microsoft Office 22/9/20 16:46
 Eliminato: through Merapi and Soufrière type... dome growths and collapses. ... [24]

330 2.3 The CVC plumbing system

331 Seismic tomography (Spica et al. 2017) highlights a 15 km-deep low velocity body (LVB), which
 332 was interpreted as the deep magma reservoir. It is confined within the CR, suggesting a structural
 333 control of the normal fault system on it (Spica et al., 2014). The LVB has an extent of ca. 55 km × 30
 334 km in the N-S and E-W directions respectively, showing an averaged thickness < 8 km. Escudero and
 335 Bandy (2017) obtained a higher resolution tomographic image of the CVC subsurface area, showing
 336 that the most active magma generation zone is now under the Fuego de Colima edifice. The ambient
 337 seismic noise tomographic study of Spica et al. (2014) indicates a shallow magma chamber above ca.
 338 7 km depth, in agreement with petrological studies (Medina-Martinez et al., 1996; Luhr, 2002; Zobin
 339 et al., 2002; López-Loera et al., 2011; Reubi et al., 2013, 2019; Maciàs et al., 2017). Cabrera-
 340 Gutiérrez and Espíndola (2010) suggested the shallow active magma storage has a volume of ca. 30
 341 km³. It is connected to the surface by conduits, whose path is facilitated by the presence of the CR
 342 fault zone, which provide a natural pathway for fluids (e.g., Allan, 1986; Norini et al., 2010, 2019).
 343 The arrangement of dykes and the alignment of volcanic centres of CVC suggest that the dykes
 344 swarm draining the magma chambers developed along the NNE-SSW-trending, steep, eastward
 345 dipping normal fault exposed on the northern CVC flank (Norini et al., 2010, 2019).

Utente di Microsoft Office 22/9/20 16:47
 Eliminato: (...017) indicate ... ighli... [25]

Silvia 19/9/20 18:24
 Eliminato: . Its horizontal extension seems to be

Utente di Microsoft Office 22/9/20 16:51
 Eliminato: appears delimited by

Silvia 19/9/20 18:23
 Eliminato: the borders of the

Antonio Costa 27/9/20 12:14
 Eliminato:

Silvia 19/9/20 18:25
 Eliminato: mean

Utente di Microsoft Office 22/9/20 16:54
 Eliminato: Also

Silvia 19/9/20 18:26
 Eliminato: in the CVC ...rea, showi... [26]

Utente di Microsoft Office 22/9/20 16:54
 Eliminato: In particular,...the ...he ... [27]

Silvia 19/9/20 18:28
 Eliminato: the presence of

Utente di Microsoft Office 22/9/20 16:55
 Eliminato: as also demonstrated...n... [28]

Silvia 19/9/20 18:29
 Eliminato: . The shallow magma chamber is

Utente di Microsoft Office 22/9/20 16:56
 Eliminato: a dyke/conduitfeeder system

Silvia 19/9/20 18:30
 Eliminato: which provides

Utente di Microsoft Office 22/9/20 16:56
 Eliminato: providing

Silvia 19/9/20 18:37
 Eliminato: Taking into account the previous information,

346 Massaro et al. (2018) provided a first-order geometrical reconstruction of the Fuego de Colima
 347 feeding system during the 1913 sub-Plinian eruption, by using volcanological data (Saucedo et al.,

428 2010, 2011; Bonasia et al., 2011) as input and constraints for numerical simulations. Results showed
 429 good matches for a hybrid configuration of the shallow conduit-feeding system composed of a ca.
 430 5500 m long, 200-2000 m wide, and 40 m width dyke passing into a shallower (500 m long, 40 m
 431 diameter) cylindrical conduit. The shallow magma chamber top was set at 6 km of depth, and dyke-
 432 cylinder transition at 500 m below the summit as inferred from geophysical data (Salzer et al., 2014;
 433 Aràmbula et al., 2018).

434
 435

436 3 Methods

437
 438 In this study, we used the commercial 8.0 version of LISA (www.lisafea.com), a general-purpose
 439 Finite Element Analysis (FEA) software developed in the '90s and based on the formulations
 440 proposed by Rao (1989), and successively integrated from other sources (Bathe, 1990; Michaeli,
 441 1991; Schwarz, 1991; Babuska et al., 1995). Despite LISA was originally used for structural analysis
 442 (Rao, 1989; 2013), it successfully predicts the stress-strain behaviour of rock masses in elastic
 443 models, in particular the deformation mechanisms even in layered rock masses (Gabrieli et al., 2015).

444 3.1 Modelling approach

445
 446 The stress field of the CVC plumbing system is simulated considering an E-W cross-section, parallel
 447 to the extension associated to the active CR (Norini et al., 2010; 2019) as shown in Figure 1a-b (a-a').
 448 Since the extent of the CVC magma chambers in the NNE-SSW direction is typically much longer
 449 than the dimensions of the E-W cross section (Spica et al., 2017), 2D solutions of either numerical or
 450 analytical models describing E-W elongated magma chambers in the crust can be reasonably adopted
 451 (Jaeger et al., 2009; Costa et al., 2011). A topographic profile and 2D plane along the chosen E-W
 452 cross-section of the CVC area was obtained in ESRI ArcGIS from a Digital Elevation Model (DEM,
 453 resolution 50 m (Instituto Nacional de Estadística y Geografía - INEGI <https://en.www.inegi.org.mx/>))

- Utente di Microsoft Office 22/9/20 18:31
Eliminato: and
- Utente di Microsoft Office 22/9/20 18:31
Eliminato: thick
- Utente di Microsoft Office 22/9/20 18:31
Eliminato: developing
- Silvia 19/9/20 18:39
Eliminato: The best-fit dyke geometry has width in the range from 200 m to 2000 m and thickness of ca. 40 m, with the cylindrical conduit diameter similar to the dyke thickness.
- Utente di Microsoft Office 22/9/20 18:33
Eliminato: in
- Silvia 19/9/20 18:41
Eliminato: also
- Silvia 19/9/20 18:44
Eliminato: software
- Silvia 19/9/20 18:44
Eliminato: . LISA is
- Silvia 16/9/20 21:50
Eliminato: . Since then, formulations from many other sources were also
- Utente di Microsoft Office 22/9/20 18:40
Eliminato: FEA
- Silvia 16/9/20 21:51
Eliminato: is also able to
- Silvia 16/9/20 21:51
Eliminato: accounting for
- Utente di Microsoft Office 22/9/20 18:35
Eliminato: and failure
- Utente di Microsoft Office 22/9/20 18:41
Eliminato: ,
- Silvia 19/9/20 18:45
Eliminato: .
- Utente di Microsoft Office 22/9/20 18:40
Eliminato: Simplifying techniques in structural FEA can give valuable insights into local stresses more rapidly and efficiently than a full 3D model. Here we considered : ... [29]
- Utente di Microsoft Office 22/9/20 18:38
Eliminato:
- Silvia 16/9/20 21:55
Eliminato: Taking into account the ... [30]
- Silvia 16/9/20 21:55
Eliminato: we simulated the
- Silvia 16/9/20 21:56
Eliminato: which is
- Silvia 16/9/20 21:56
Eliminato: Colima Rift
- Silvia 16/9/20 21:56
Eliminato: ,
- Silvia 16/9/20 22:04
Eliminato: ;
- Silvia 16/9/20 22:04
Eliminato: m;

498 and imported into Autodesk Auto-Cad R13 using a third-degree spline approximation. The IGES file
499 was then imported into LISA for the mesh discretization.

500 The investigated domain extends 60 x 30 km in a x-z Cartesian Coordinate System with a three and
501 four-node finite element discretization (Table 1). Zero normal displacements are assigned at the
502 bottom and the lateral boundaries, while the upper boundary represents the free-stress ground surface
503 (Fig. 1c). The FEM is carried out by using a plane strain approximation, implying that the
504 deformation in the third direction is assumed to be negligible.

505 As reported in Zehner et al. (2015), FEM of geological structures requires accurate discretization of
506 the computational domain. It follows that the unstructured tetrahedral meshes has to fulfil the
507 following requirements: i) sufficient mesh quality: the tetrahedrons should not be too acute-angled,
508 since numerical instabilities can occur, ii) incorporation of geometry for defining boundary
509 conditions and constraints, iii) local adaption, which is a refinement of the mesh in the vicinity of
510 physical sources in order to avoid numerical errors during the simulation. In this work we adopted a
511 mesh composed of 4660 plane continuum elements, which have been refined in the regions of higher
512 gradients (i.e. near the contours of the magmatic feeding system).

513 In our simulations, the extent of the rock layers (Table 2) is referred to Norini et al. (2010, 2019). The
514 configuration of the CVC feeding system (i.e. depth, shape and dimensions of the magma chambers
515 and feeder dykes) derives from the literature (Spica et al., 2014, 2017; Massaro et al., 2018, 2019)
516 and it is simplified in Figure 1d. In particular, magma chambers and dykes are considered as
517 pressurized finite-size bodies in an elastic crustal segment, acting as fluid-filled holes. The boundary
518 condition (pressurization) is provided by applying internal forces that act on the walls. This approach
519 has been extensively used in several analytical and numerical models that treat magma reservoirs as
520 internally pressurized ellipsoidal cavities within an elastic half space, in order to gain insight into the
521 behaviour of magma plumbing systems (Pinel and Jaupart, 2004; Gudmundsson, 2006; Grosfils,
522 2007; Andrew and Gudmundsson, 2008; Hautmann et al., 2013; Currenti and Williams, 2014; Zhong
523 et al., 2019).

524 Previously published studies indicate that differences between, and problems with, elastic models
525 derive principally from the key role played by gravity (e.g. Albino et al., 2018; Gerbault, 2012; Lister
526 and Kerr, 1991; Watanabe et al., 2002). Some authors argued on whether it is appropriate or not to

Silvia 16/9/20 22:00
Eliminato: . This cross section was ... [31]

Silvia 19/9/20 18:48
Eliminato: performed. The domain was discretized by three and four-node finite elements (Table 1; Fig. 1c). ...he inve... [32]

Utente di Microsoft Office 22/9/20 18:43
Eliminato: analysis

Silvia 19/9/20 19:01
Spostato (inserimento) [2]

Utente di Microsoft Office 22/9/20 18:44
Eliminato:

Silvia 19/9/20 19:02
Eliminato: such that geological units are represented correctly. Zehner et al. (2015) reported that

Silvia 19/9/20 19:01
Spostato in su [2]: Zehner et al. (2015)

Utente di Microsoft Office 22/9/20 18:44
Eliminato: therefore

Silvia 19/9/20 19:03
Eliminato: on a complex geological ... [33]

Silvia 16/9/20 22:10
Eliminato: the model of

Utente di Microsoft Office 22/9/20 18:46
Eliminato: complete geometrical ... [34]

Silvia 19/9/20 19:18
Eliminato: M

Silvia 19/9/20 19:18
Eliminato: The geometrical configuration set for the CVC feeding system (i.e. the shape and dimensions of the magmatic chambers) derives from the literature (Spica et al., 2014, 2017; Massaro et al., 2018, 2019) and it is simplified in Figure 1d. The overpressure in magma chambers may be produced by a variety of processes, including fractional crystallization, volatile exsolution and magma recharge, leading to deviatoric stresses in the country rock that may be tens of MPa in magnitude (Jellinek and DePaolo, 2003; Karlstrom et al., 2010).

Silvia 16/9/20 22:13
Spostato in giù [1]: The overpressure in magma chambers may be produced by a variety of processes, including fractional crystallization, volatile exsolution and magma recharge, leading to deviatoric stresses in the country rock that may be tens of MPa in magnitude (Jellinek and DePaolo, 2003; Karlstrom et al., 2010).

Utente di Microsoft Office 22/9/20 18:48
Eliminato:) that. Gravity plays a first order role on bedrock failure conditions (... [35]

634 account for the gravity body force in models of volcanic systems (e.g. Currenti and Williams, 2014;
635 Grosfils et al., 2015). When the gravitational loading is not included in the model, the volcanic
636 deformation results from a change with respect to a stage previously at equilibrium (e.g. Gerbault et
637 al. 2018). In this work, we carried out simulations considering the effect of the gravitational loading
638 in the host rock, implemented via body forces. The model initial condition has a pre-assigned
639 lithostatic stress, whose computation, in presence of topography and material heterogeneities, is not
640 trivial because it requires applying the gravity load preserving the original not deformed geometry of
641 the mesh (Cianetti et al., 2012). Since the presence of a lithostatic stress field, the load applied at the
642 reservoir boundaries represents a superposition of the magmatic pressure and lithostatic component.
643 *We define here the magmatic pressure as either excess pressure (ΔP_g , magmatic minus lithostatic*
644 *pressure but below the tensile strength of wall rocks) or over pressure (or driving pressure ΔP_g ,*
645 *which is the magmatic pressure exceeding tensile strength of wall rocks; Gudmundsson, 2012). The*
646 *first pertains to the FEMs using isolated magma chambers (single or double), while the second is*
647 *used for models with connected magma chambers (with conduit/feeding system).*
648 We also took into account the effect of the existing faults of the CR system even if LISA cannot
649 include a frictional law to represent the fault movement (i.e. Chaput et al., 2014). As reported in
650 Jeanne et al. (2017 and reference therein) the damage induced by faults increases from the host rocks
651 to the fault core, implying the reduction in the effective elastic moduli. *In this light*, we represented
652 the faults bordering the CR as two damage zones (ca. 70° of inclination, ca. 1 km thick, and down to
653 10 km of depth) showing reduced elastic properties with respect to the surrounding host rocks.
654 *To take into account the effect of far field extensional regime, we applied a uniform stress of 5 MPa*
655 *to the lateral boundaries of the domain (as reported in Marti and Geyer, 2009).*
656 *Considering the E-W cross-section (a-a'; Fig. 1a), we provided six domain configurations: i)*
657 *“homogeneous lithology model” in which the volcanic domain is only composed of andesite rocks; ii)*
658 *“not homogeneous lithology model” where different geological units are considered; iii) “single*
659 *magma chamber model” composed of a not homogeneous lithology and a 15 km-deep magma*

- Silvia 16/9/20 22:15
Eliminato: numerical
- Utente di Microsoft Office 22/9/20 18:50
Eliminato: inflation
- Silvia 19/9/20 19:23
Eliminato: . Gravity ...n the host ro ... [36]
- Utente di Microsoft Office 25/9/20 11:44
Eliminato: over...ressure ... [37]
- Silvia 28/9/20 09:59
Eliminato:
- Silvia 28/9/20 09:59
Formattato: Non Apice/ Peditice
- Silvia 28/9/20 09:59
Eliminato:
- Silvia 28/9/20 10:00
Formattato: Non Apice/ Peditice
- Silvia 28/9/20 09:59
Eliminato: ...which is the magmati ... [38]
- Utente di Microsoft Office 25/9/20 11:49
Formattato: Tipo di carattere:Symbol
- Antonio Costa 27/9/20 12:24
Formattato: Tipo di carattere:(Predefinito)
Times New Roman, Peditice
- Silvia 28/9/20 10:03
Eliminato: T...e second is used for ... [39]
- Silvia 28/9/20 10:03
Formattato ... [40]
- Utente di Microsoft Office 22/9/20 19:55
Eliminato: Colima Graben (CG)...F ... [41]
- Silvia 19/9/20 19:25
Eliminato: Considering the evaluation of
fault zone elastic properties provided by
Jeanne et al. (2017)
- Utente di Microsoft Office 22/9/20 19:55
Eliminato: CG ...R as two damage ... [42]
- Silvia 19/9/20 19:25
Eliminato: down
- Utente di Microsoft Office 22/9/20 18:57
Eliminato: up to 10 km in depth
- Utente di Microsoft Office 22/9/20 21:58
Formattato: Spazio Dopo: 12 pt
- Silvia 25/9/20 14:19
Eliminato: of
- Antonio Costa 27/9/20 12:27
Eliminato: n
- Silvia 25/9/20 14:20
Eliminato: at

706 chamber; iv) “*dual magma chamber model*” composed of a not homogeneous and 6 km- and 15 km-
707 deep magma chambers; v) “*conduit feeding system model*” composed of not homogeneous lithology,
708 6 km- and 15 km-deep magma chambers connected through a deep dyke evolving into a shallow
709 conduit near the surface; vi) “*extensional model*”, with a 5 MPa horizontal extensional stress (far
710 field) and, vii) “*faulted model*”, in which are also added two damaged zones mimicking the CR faults
711 (local stress) (Fig. 1b).

712 The number of nodes in the only substratum and single magma chamber models is set at 4426, for the
713 dual magma chamber model is set at 4161, and at 3737 for the conduit feeding system and faulted
714 models.

715 It is important to note that simulations outputs are shown using different colour scales. Although
716 such a choice may result into a difficult visual comparison of the different runs, it preserves the
717 necessary details of stress distribution, which would have been lost using a common colour scale.

718 Finally, in the following we refer to σ_1 as the greatest compressive stress and σ_3 is the least
719 compressive stress.

722 4 Geological data

724 4.1 Stratigraphy and rock mechanics

725 Four units forming the CVC system are defined from the available geological data (Table 2): i)
726 Basement (Unit B): cretaceous limestones and intrusive rocks forming the bed-rock underlying the
727 CVC; ii) Graben fill deposits (Unit GF): Quaternary alluvial, colluvial, and lacustrine deposits filling
728 the graben; iii) Fuego de Colima deposits (Unit FC): andesitic lavas and pyroclastic deposits forming
729 the Paleofuego-Fuego de Colima edifices; and iv) Volcaniclastic deposits (Unit VD): volcaniclastic
730 deposits covering the southern flank of the CVC (e.g. Cortés et al. 2010; Norini et al., 2010, 2019).

Utente di Microsoft Office 22/9/20 22:20
Formattato: Livello 1, Spazio Dopo: 10 pt, Controlla righe isolate

Utente di Microsoft Office 22/9/20 22:20
Formattato: Tipo di carattere:(Predefinito) Times, Colore carattere: Automatico

Silvia 16/9/20 22:21
Eliminato: we chose to represent the different

Utente di Microsoft Office 22/9/20 18:59
Eliminato: the results from

Utente di Microsoft Office 22/9/20 18:59
Eliminato: implies a

Silvia 19/9/20 19:26
Eliminato: makes more

Silvia 19/9/20 19:26
Eliminato: a

Silvia 19/9/20 19:26
Eliminato: of the simulation

Utente di Microsoft Office 22/9/20 19:00
Eliminato: model outputs

Silvia 16/9/20 22:22
Eliminato: and it needs to be kept in mind looking at the different figures

Silvia 16/9/20 22:22
Eliminato: for all the figures in LISA.

Antonio Costa 27/9/20 12:28
Formattato: Tipo di carattere:(Predefinito) Times New Roman, 12 pt, Pedice

Antonio Costa 27/9/20 12:29
Formattato: Tipo di carattere:(Predefinito) Times New Roman, Pedice

Silvia 27/9/20 21:21
Eliminato: .

Silvia 19/9/20 19:27
Eliminato: In this work, we used geological information available in literature as input data, in order to estimate the stress variations around the CVC magmatic plumbing system. Here we briefly describe the main geological features taken into account in LISA simulations. .

Silvia 19/9/20 19:28
Eliminato: were

Silvia 19/9/20 19:33
Eliminato: Being the area interested by FEM extended down to 30 km, it is evident how Unit B is dominant with respect to the others, which occupy only few km in the upper part of the simulated domain.

756 We assumed constant mechanical characteristics within each Unit using the typical rock mass
 757 properties, density (ρ), Young Modulus (E) and Poisson Ratio (ν) (Table 2). The rock masses are
 758 considered dry, in order (eventual) pore pressure to be neglected. Only for Unit GF a higher value for
 759 the Poisson Ratio was used close to the surface in order to mimic high water content in the graben
 760 sediments. The maximum thickness of the graben fill (about 1 km) is assumed from the literature
 761 (Allan, 1985; Serpa et al., 1992; Norini et al., 2010, 2019). For Units B and GF rock mass proprieties
 762 are derived from Hoek and Brown (1997) and Marinos and Hoek (2000), while for volcanic materials
 763 (units FC and VD; Table 2) are estimated according to the approach proposed by Del Potro and
 764 Hürlimann (2008). In order to describe the effects of the CR faults on stress field distribution, the
 765 mechanical properties are locally degraded in proximity of the faults themselves.

767 4.2 The geometry of the plumbing system

768 In our 2D model, we assume the CVC composed of a two magma chambers connected by dykes and
 769 to the surface by a conduit (Fig. 1d). The shape of the magma chambers and dykes are represented by
 770 elliptical cross-sections with the major ($2a$) and minor ($2b$) axes.

771 Generally, the magma chambers have a sill-like shape that is often imaged in seismic studies of
 772 volcanoes and rift zones (Macdonald, 1982; Sinton and Detrick, 1992; Mutter et al., 1995; MacLeod
 773 and Yaouancq, 2000; Singh et al., 2006; Canales et al., 2009). Most of them are not totally molten but
 774 rather a mixture of melt and crystal mush (i.e. Parfitt and Wilson, 2008). Various estimates have been
 775 made to infer the actual amount of melt in a magmatic body, showing that it is only ca. 10% of the
 776 total chamber volume (Gudmundsson et al., 2012 and reference therein).

777 After Spica et al. (2017), the 15 km-deep LVB is ca. 7000 km³, therefore, if we assume
 778 10%, the deep magma chamber volume would be ca. 700 km³. Simplifying this volume in an
 779 elliptical sill-like geometry, the magma chamber dimensions (i.e. $2a$, $2b$, $2c$ axes) have to be scaled
 780 according to the LVB ($55 \times 30 \times 8$ km; Spica et al., 2017) using $2a = 14$ km, $2b = 3.6$ km, $2c = 26$
 781 km, being $2c$ elongated in NW-SE direction. For the shallow part of the feeder system, we have no
 782 detailed geophysical constraints. However, Massaro et al. (2019) reproduced through numerical
 783 modelling the nonlinear cyclic eruptive activity at Fuego de Colima in the last 20 years, using a

Silvia 19/9/20 19:30
Spostato in giù [3]: We assumed constant mechanical characteristics within each Unit (Table 2).

Silvia 19/9/20 19:30
Eliminato: We assumed constant mechanical characteristics within each Unit (Table 2). In particular, Unit B was co... [43]

Utente di Microsoft Office 22/9/20 19:48
Eliminato: Deformation within the brittle upper crust is described by elastic material's behaviour.

Silvia 19/9/20 19:30
Spostato (inserimento) [3]

Silvia 19/9/20 19:30
Eliminato: (Table 2). For each Unit we fixed

Silvia 19/9/20 19:36
Formattato: Spazio Dopo: 0 pt

Utente di Microsoft Office 22/9/20 19:51
Eliminato: 's...Modulus (E) and ... [44]

Silvia 19/9/20 19:34
Eliminato: was ...s assumed from th... [45]

Utente di Microsoft Office 22/9/20 19:53
Eliminato: This information allowed Norini et al. (2019) to derive the equivalent Mohr-Coulomb properties for the stress ranges expected in the different sectors of the CVC.

Silvia 19/9/20 19:35
Eliminato: In addition, ...i ... [46]

Utente di Microsoft Office 22/9/20 19:54
Eliminato: CG

Silvia 19/9/20 19:35
Eliminato: were

Silvia 19/9/20 19:37
Eliminato: The geometry of the E-W cross-section of the CVC plumbing system was modelled taking into account the previous subsurface information described in Section 4.1.

Utente di Microsoft Office 22/9/20 19:59
Eliminato: Considering

Silvia 19/9/20 19:39
Eliminato: with its top at ca. 15 km of depth and with an estimated volume of ...a... [47]

858 shallow magma chamber volume in the range of 20-50 km³, according to the estimation of Cabrera-

859 Gutiérrez and Espindola (2010). Here we assume a volume of 30 km³, using 2a = 3.5 km, 2b = 2 km,

860 2c = 8 km as dimensions of the shallow magma chamber.

861 Numerous theoretical and field studies have established that host rock stresses dictate the magma-

862 pathways (e.g. Maccaferri et al., 2011; Gudmundsson, 2011). During ascent to the surface, the dykes

863 align themselves with the most energy-efficient orientation, which is roughly perpendicular to the

864 least compressive stress (e.g. Gonnermann and Taisne, 2015; Rivalta et al., 2019), providing the

865 magma driving pressure remains small compared to the deviatoric stress (Pinel et al., 2017;

866 Maccaferri et al., 2019). This behaviour, however, can be modulated in the presence of significant

867 variations in fracture toughness of the surrounding rock due to stratification (Maccaferri et al., 2010)

868 or to old and inactive fracture systems (Norini et al., 2019).

869 Although for oblate magma chambers the propagation of dykes is most probable from the tip areas, in

870 our simulations the orientation of dykes is assumed vertical, because of the preferential pathways

871 represented by the CR fault planes (Spica et al., 2017).

872 We set the dimensions of feeder dykes in agreement with Massaro et al. (2018): deep dyke 2ad = 2

873 km; shallow dyke 2a varies from 1 km at bottom to 500 m in the upper part of the volcano; width of

874 both deep and shallow dyke 2bd = 2b = 100 m (Fig. 1d).

875 It is worth noting that it is outside the scope of this work providing the conditions for the magma

876 chamber rupture, being LISA accounting only for the elastic regime. For these reasons, we fixed ΔP_e

877 and ΔP_c (for isolated and connected magma chamber models, respectively) in the range of 10 - 20

878 MPa for the 15 km-deep chamber, and 5 MPa for the 6 km-deep one. For the dykes and conduit, ΔP_c

879 is set to 10 MPa in the deeper dyke and 5 MPa in the shallower one, while in the upper 500 m of

880 conduit is 0.4 MPa.

881

882

883 **5 Results**

884

Silvia 19/9/20 19:45
Eliminato: also ...cording to the es... [48]

Utente di Microsoft Office 22/9/20 20:21
Eliminato: .

Silvia 19/9/20 19:52
Formattato: Spazio Dopo: 0 pt

Silvia 16/9/20 19:14
Eliminato: the least compressive principal stress axis

Utente di Microsoft Office 22/9/20 20:06
Eliminato: σ ... (e.g. Gonnermann : ... [49]

Silvia 16/9/20 19:18
Eliminato: Although, for decades, magma conduits were modelled as cylinders, because of easiness of their mathematical treatment, geophysical data and field observations highlight the importance and peculiarities of dykes in magma transport and hence the need to adopt more realistic geometries (Costa et al., 2009; Hautmann et al., 2013; Tibaldi, 2015). It is important to stress that

Utente di Microsoft Office 22/9/20 20:13
Eliminato: Although all cavities/inclusions in a medium modify the local stress field and concentrate stresses, the induced perturbation depends mainly on the geometry of the cavity/inclusion (Savin, 1961; Borelli et al., 1985; Tan, 1994; Saada, 2009). Geophysical data and field observations highlighted the importance and peculiarities of dykes in magma transport and hence the need to adopt more realistic geometries for magma pathways (Costa et al., 2009; Hautmann et al., 2013; Tibaldi, 2015). We Here w

Silvia 19/9/20 19:56
Eliminato: , although the exact value of the latter is not crucial for the purposes of this study. Moreover, ... is worth notin... [50]

Utente di Microsoft Office 22/9/20 20:13
Eliminato: e

Silvia 19/9/20 19:57
Eliminato: to provide

Utente di Microsoft Office 25/9/20 11:58
Eliminato: the selected magma overpressures (ΔP) acting on the magma reservoirs chambers and dykes have to be less than the tensile strength of the rocks. We therefore fixed

Antonio Costa 27/9/20 12:38
Formattato ... [51]

Silvia 19/9/20 19:58
Eliminato: at ...0 - MPa and ... [52]

Antonio Costa 27/9/20 12:39
Formattato ... [53]

Utente di Microsoft Office 22/9/20 20:14
Eliminato:

Silvia 19/9/20 19:59
Eliminato: the magmatic overpressure is fixed at ...0 MPa in the deeper dyke a... [54]

Utente di Microsoft Office 22/9/20 21:57
Eliminato: To take into account the effect of both far field extensive regime and ... [55]

L002 In this section we reported the sensitivity analysis carried out to quantify the approximation of the
 L003 Young Modulus variation on FEM outputs, and the description of the model outputs when adding
 L004 complexity to the input geological/geophysical data.

L006 5.1 Sensitivity analysis of Young Modulus

L007 Using the single magma chamber model as reference case, we quantified the influence of the Young
 L008 Modulus variation in each geological Units. Taking into account the mechanical properties of rocks
 L009 (Table 2) as reference values, we compared the stress state of the computational domain at changing
 L010 Young Modulus by (\pm) an order of magnitude. This sensitivity analysis, although incomplete, may
 L011 lead to raise awareness on the selection of input data when running a FEM. The sensitivity analysis
 L012 was carried out on a reduced simulation domain (the x -axis was set to 35 km) in order to diminish the
 L013 influence of binding effects along the domain borders.
 L014 We applied the Euclidean norm (L2) method for illustrating the results. The L2 norm applied on a
 L015 vector space x (having components $i = 1, \dots, n$) is strongly related with the Euclidean distance from its
 L016 origin, and is equal to:

$$L018 \quad ||x||_2 = \sqrt{\sum_i^n x_i^2} \quad (1)$$

L020 In our case, the vector space x is composed of all nodes of the computational domain (Table 1). We
 L021 defined x_{ref} the vector containing the results for the maximum and minimum principal stress when
 L022 using the selected values of material properties (Table 1) and $x(-)$, $x(+)$ the vectors at varying the
 L023 Young Modulus of one order of magnitude in each Unit.

L024 In Figure 2 are reported the global relative variations in L2 of σ_1 and σ_3 caused by the variation of
 L025 Young Modulus in each Unit, for each model configuration (i.e. not homogeneous lithology, single
 L026 magma chamber, dual magma chamber, and dual magma chamber with conduits models) as follow:

$$L028 \quad L2(-) = \frac{||x_{ref} - x(-)||_2}{||x_{ref}||_2} \quad (2)$$

Silvia 16/9/20 19:43
Eliminato: The first part of this section is focused on a ...ensitivity analysis of Y... [56]

Utente di Microsoft Office 22/9/20 22:01
Eliminato: 's

Silvia 16/9/20 19:53
Eliminato: this important rock prop... [57]

Utente di Microsoft Office 22/9/20 22:04
Eliminato: Considering the E-W cross-section (a-a'; Fig. 1a), we provided six domain configurations with increasing geological complexity: i) "homogeneous lithology model" in which the volcanic domain is only composed of andesite rocks; ii) "not homogeneous lithology model" where different geological units are considered; iii) "single magma chamber model" composed of a not homogeneous lithology and a 15 km-deep magma chamber; iv) "dual magma chamber model" composed of a not homogeneous and 6 km- and 15 km-deep magma chambers; v) "conduit feeding system model" composed of not homogeneous lithology, 6 km- and 15 km-deep magma chambers connected through a deep -dyke evolving into, and a shallow conduit connecting (tonear the surface; vi) "extensional model", with a in which we added a 5 MPa horizontal extensionaextensiv stress (far field) and, vii) "faulted model", in... [58]

Silvia 19/9/20 20:11
Eliminato: In order to quantify the influence of Young Modulus selection on the m... [59]

Utente di Microsoft Office 22/9/20 22:21
Eliminato: 's

Silvia 19/9/20 20:10
Eliminato: ...odulus variation in ea... [60]

Utente di Microsoft Office 22/9/20 22:22
Eliminato: rock...echanical 's... [61]

Silvia 19/9/20 20:11
Eliminato: used in the simulations (Norini et al., 2010, 2019; Table 2)

Utente di Microsoft Office 22/9/20 22:22
Eliminato: in... ..able 2) as referen... [62]

Silvia 19/9/20 20:12
Eliminato: ...odulus by (\pm) an orde... [63]

Silvia 19/9/20 20:15
Eliminato: used ...plied the Euclid... [64]

Silvia 20/9/20 00:25
Formattato: Tipo di carattere:8 pt

Utente di Microsoft Office 22/9/20 22:23
Eliminato: 's

Silvia 19/9/20 20:16
Eliminato:

Silvia 19/9/20 20:19
Spostato (inserimento) [4]

Silvia 20/9/20 00:16
Eliminato: the principal maximum s... [65]

Utente di Microsoft Office 22/9/20 22:24
Eliminato: 's

Silvia 19/9/20 20:19
Eliminato: . . . [66]

L178
$$L_2(+) = \frac{\|x_{ref} - x(+)\|_2}{\|x_{ref}\|_2} \quad (3)$$

L179
 L180 All the **models** show variability less than 15%, with few exceptions within Unit B that have
 L181 variability over 30% (Fig. 2). **In this light**, the spatial distribution of the major variations seems to not
 L182 significantly affect the final stress distributions, because: i) they are located near the mesh borders
 L183 (Fig. 3a, b); and, ii) when not at the mesh borders, the variations are limited to few % (Fig. 3c, d). It
 L184 means that **the one order of magnitude variation in** Young Modulus produces variation in FEM
 L185 outputs distributed over a large domain, and the change affecting the single nodes is limited to few %.

L187 *5.2 Homogeneous and not homogeneous lithology*

L188 In Figure 4 we reported **σ_1 and σ_3 stresses for gravity loaded models with homogeneous lithology**
 L189 **composed by only andesitic lavas (Fig. 4a) and not homogeneous lithology composed of carbonates**
 L190 (Unit B), alluvial, volcanoclastic and pyroclastic deposits (Units GF and VD; Fig. 4b). It is
 L191 important to stress that the $x-z$ zero displacement assigned at the bottom and **at** the lateral boundaries
 L192 of the domain created substantial artefacts in the results (i.e. curved patterns of stress), **especially**
 L193 **considering σ_3 (Fig. 4, panels i-ii)** where the boundary effect on x -axis is amplified by the presence of
 L194 the upper free surface. **It follows that** the only unperturbed **area** extends ca. 30 km horizontally and ca.
 L195 15 km vertically (within the blue contour in Fig. 4). **It is worth noting that the homogeneous and not-**
 L196 **homogeneous models show quite similar results in stress patterns (Fig. 4).**

L198 *5.3 Gravitational modelling using the inferred feeding system geometry*

L199 In Figures 5 and 6 we show three cross-section profiles **describing** the feeding system starting from a
 L200 single to two magma chambers, then adding the conduits, and, finally, considering the **full**
 L201 **complexity by adding the effects of far-field stress and CR faults**. Figure 5a describes **σ_3 (panel i)**
 L202 **and σ_1 (panel ii) stress distribution for the single magma chamber model, and $\Delta P_e = 10$ MPa**. No
 L203 significant differences in magnitude and pattern of stresses are visible **using $\Delta P_e = 20$ MPa**
 L204 (Appendix 1a).

L205 The addition of the shallow magma chamber significantly changes the values and pattern of both σ_3

Spostato in su [4]: In Figure 2 ar... [67]

Utente di Microsoft Office 22/9/20 22:24
 Eliminato: geometrical configurations

Silvia 19/9/20 20:21
 Eliminato: It is worth noting that... [68]

Utente di Microsoft Office 22/9/20 22:25
 Eliminato: 's

Silvia 19/9/20 20:22
 Eliminato: of one order of magnitude

Silvia 20/9/20 00:23
 Eliminato: We carried out LISA sin... [69]

Utente di Microsoft Office 22/9/20 22:27
 Eliminato: a ...ravity loading ...oad... [71]

Silvia 20/9/20 00:34
 Eliminato: ...lithology rock compo... [72]

Antonio Costa 27/9/20 12:44
 Formattato ... [70]

Utente di Microsoft Office 22/9/20 22:27
 Eliminato: the ...ot- ...omogeneous... [73]

Silvia 20/9/20 00:34
 Eliminato: by

Utente di Microsoft Office 22/9/20 22:28
 Eliminato: ...showing a . We analy... [74]

Silvia 20/9/20 00:37
 Eliminato: very ...mportant to stres... [75]

Antonio Costa 27/9/20 12:45
 Formattato ... [76]

Silvia 20/9/20 00:39
 Eliminato: For this reason, ...he onl... [77]

Utente di Microsoft Office 22/9/20 22:32
 Eliminato: which

Silvia 20/9/20 00:38
 Eliminato: , and it

Silvia 20/9/20 00:41
 Eliminato: We progressively add th... [78]

Antonio Costa 27/9/20 12:47
 Eliminato: are...shown ... [79]

Silvia 20/9/20 00:41
 Eliminato: T

Utente di Microsoft Office 22/9/20 22:38
 Eliminato: (Figs. 5, 6)

Silvia 20/9/20 00:41
 Eliminato: show increasing complexity of

Utente di Microsoft Office 22/9/20 22:38
 Eliminato: fedeer

Silvia 20/9/20 00:42
 Eliminato: magma chamber, passing

Utente di Microsoft Office 22/9/20 22:38
 Eliminato: G

Silvia 20/9/20 00:43
 Eliminato: the distribution of the mi... [80]

Antonio Costa 27/9/20 12:47
 Formattato ... [81]

Silvia 20/9/20 00:43
 Eliminato: the maximum principal stress

Antonio Costa 27/9/20 12:48
 Formattato ... [82]

Silvia 20/9/20 00:45
 Eliminato:

Utente di Microsoft Office 22/9/20 22:40
 Eliminato: in a

Silvia 20/9/20 00:44
 ... [83]

Utente di Microsoft Office 22/9/20 22:40
 ... [84]

Silvia 25/9/20 14:26
 Formattato ... [85]

Utente di Microsoft Office 22/9/20 22:40
 ... [86]

Silvia 25/9/20 14:26
 Formattato ... [87]

Silvia 20/9/20 09:49
 ... [88]

L330 and σ_1 (Fig. 5b). In particular, σ_3 and σ_1 stresses describe a typical inflation pattern produced by
L331 excess pressure in magma chamber(s) (Anderson, 1936; Gudmundsson, 2006; 2012), producing well-
L332 defined stress arches of σ_3 (red dotted lines in Figs. 5bi) and divergent strong gradients of σ_1 around
L333 the deep magma chamber (Fig. 5bii). Very slight differences in magnitude and pattern of stresses
L334 appear when using $\Delta P_e = 10$ MPa (Fig. 5b) or 20 MPa (Appendix 1b).

L335 Looking at Figure 6 it is evident how the insertion of the conduits in the CVC feeding system
L336 dramatically changes the stress distribution, with the disappearance of the stress arch and a nearly
L337 constant stress in the computational domain except around the deep magma chamber tips.

L339 5.4 Application of an extensional stress field

L340 In order to explore the influence of the extensional far field stress on stress patterns (Fig. 1a), we run
L341 simulations applying 5 MPa stress (typical low value for rift zones; Turcotte and Schubert, 2002;
L342 Moeck et al., 2009; Maccaferri et al., 2014; Sulpizio and Massaro, 2017) along the lateral boundaries
L343 of the computational domain (Fig. 7).

L344 In the case of a single magma chamber ($\Delta P_e = 10$ MPa; Fig. 7, panels i-ii), the addition of the far
L345 field stress reduces the confinement effect due to the no displacement condition imposed along the x -
L346 z directions (plane strain approximation). When considering the double magma chamber
L347 configuration ($\Delta P_e = 10$ MPa in the deep chamber and $\Delta P_e = 5$ MPa in the shallower one), the
L348 presence of the far field stress produces slight changes in stress magnitude and pattern for both σ_3
L349 and σ_1 (Fig. 7, panels iii-iv) with respect to Figure 5b. Very similar effects appears on the complete
L350 feeding system configuration model (Fig. 7, panels v-vi). Also in this case using $\Delta P_e = 20$ MPa in
L351 the deep magma chamber does not significantly affect the model outputs (Appendix 2).

L353 5.5 Faults bordering the Colima Rift

L354 The effect of faults bordering the CR on the final feeding system configuration is simulated through
L355 two damage zones by degrading their elastic properties. Adding these elements does not significantly
L356 alter the stress distribution observed in Figures 7v and 7vi, but only provide a slight reduction in both

Eliminato: overpressurised
Silvia 20/9/20 09:49
Eliminato: , well developed ...round ... [89]
Silvia 16/9/20 22:13
Spostato (inserimento) [1] ... [91]
Utente di Microsoft Office 22/9/20 22:45
Eliminato: It is known that stress ar ... [90]
Silvia 20/9/20 09:46
Eliminato: Stress arch is a common ... [92]
Utente di Microsoft Office 22/9/20 22:46
Eliminato: around the deep magma chamber
Utente di Microsoft Office 22/9/20 22:46
Eliminato: equal to
Silvia 20/9/20 09:48
Eliminato: MPa ...Fig. 5b) or 20 M ... [94]
Silvia 25/9/20 14:29
Formattato ... [93]
Silvia 20/9/20 10:04
Eliminato: of CVC ...ramatically cl ... [95]
Utente di Microsoft Office 22/9/20 22:47
Eliminato: 's
Silvia 20/9/20 10:07
Eliminato: .
Utente di Microsoft Office 22/9/20 22:49
Eliminato: Extensional ...xtensional ... [96]
Silvia 20/9/20 10:08
Eliminato: stress ...n stress patterns ... [97]
Utente di Microsoft Office 22/9/20 22:51
Eliminato: using
Silvia 20/9/20 10:09
Eliminato: of extensional stress to th ... [98]
Utente di Microsoft Office 22/9/20 22:51
Eliminato: as
Silvia 20/9/20 10:09
Eliminato: , which is a
Utente di Microsoft Office 22/9/20 22:51
Eliminato: (
Silvia 20/9/20 10:10
Eliminato: ; Fig. 7
Utente di Microsoft Office 22/9/20 22:52
Eliminato: ,
Silvia 20/9/20 10:10
Eliminato: ...long the lateral bound ... [99]
Silvia 25/9/20 14:30
Formattato ... [100]
Silvia 20/9/20 10:11
Eliminato: with ...0 MPa overpres ... [101]
Silvia 25/9/20 14:30
Formattato ... [102]
Silvia 20/9/20 10:12
Eliminato: with... ...0 MPa overp ... [103]
Silvia 25/9/20 14:30
Formattato ... [104]
Silvia 20/9/20 10:14
Eliminato: The same applies also f ... [105]
Utente di Microsoft Office 22/9/20 22:53
Eliminato: I... this case , also ... [106]
Silvia 20/9/20 10:17
Eliminato:U ... [107]
Silvia 20/9/20 10:18
Eliminato: overpressure
Silvia 25/9/20 14:30
Formattato ... [108]
Silvia 20/9/20 10:21
... [109]

L473 σ_1 and σ_3 intensities around their edges (Figs. 7vii and 7viii). The different distance of the two
L474 damage zones from the feeding system produces a small asymmetry in both σ_1 and σ_3 patterns with
L475 respect to simulations without damage zones, especially near the deep magma chamber (Figs. 7v-viii).

L476
L477

L478 6 Discussions

L479

L480 6.1 FEM analysis at increasing geological details

L481 This study highlights some important features of crustal stress distribution at changing geological and
L482 geophysical constraints as input conditions (Spica et al., 2014, 2017; Massaro et al., 2018). Although
L483 the results have to be considered as a first order approximation, the changes in stress distribution are
L484 appreciable and useful for a better understanding of the FEM limitations and advantages.

L485 Under the assumptions of plane strain and gravitational loading, the use of homogeneous or not
L486 homogeneous lithology provides negligible effects in stress intensity and pattern (Fig. 4). This is
L487 likely due to the limited thickness of the shallow Units (Units FC, VD, GF; Table 2) in the simulated
L488 domain, which results dominated by Unit B (Table 2). However, this does not mean that the influence
L489 of the upper Units may be still negligible using smaller scales of the simulated domain.

L490 Analysing the single magma chamber model outputs, it emerges how the ΔP_e limited the effects of
L491 gravitational loading. On the contrary, the dual magma chamber geometry better describes the
L492 inflation induced by the ΔP_e within magma chambers, with the formation of the stress arch in the σ_3
L493 plot. It is worth noting that for both single and dual magma chamber models, the ΔP_e change from
L494 10 to 20 MPa slightly affects the magnitude of the stress but not its general pattern (Appendix 1-2).

L495 The presence of dykes in the magma feeding system dramatically change the σ_3 and σ_1 patterns (Fig.
L496 6). which become quite homogeneous throughout the computational domain, with the only exception
L497 of sidewall effects induced by the zero displacement conditions.

L498 The addition of extensional field stress of 5 MPa reduces the sidewall effects and produces an almost
L499 homogeneous stress distribution in the upper part of the computational domain, above the top of the
L500 deep magma chamber. This, along with the additional inclusion of the damage zones introduced to

Eliminato: values ...ntensities in th... [110]
Utente di Microsoft Office 22/9/20 22:54
Eliminato: feeder
Silvia 20/9/20 10:31
Eliminato: (especially the deep ma... [111]
Silvia 20/9/20 10:35
Eliminato: The presented FEM mc... [112]
Utente di Microsoft Office 25/9/20 12:09
Eliminato: ...gravitational loading... [113]
Silvia 20/9/20 10:36
Eliminato: for FEM
Utente di Microsoft Office 25/9/20 12:09
Eliminato: ,
Silvia 20/9/20 10:38
Eliminato: ...the limited thickness... [114]
Utente di Microsoft Office 23/9/20 21:24
Eliminato: upper
Silvia 20/9/20 10:39
Eliminato: represent only a limited... [115]
Utente di Microsoft Office 23/9/20 21:25
Eliminato: that...hich results entir... [116]
Silvia 20/9/20 10:48
Eliminato: FEM outputs with the
Utente di Microsoft Office 23/9/20 21:26
Eliminato: 's
Silvia 25/9/20 14:31
Formattato ... [117]
Utente di Microsoft Office 25/9/20 12:11
Eliminato: overpressures, ΔP , only
Silvia 20/9/20 10:51
Eliminato: The use of...n the contr... [118]
Utente di Microsoft Office 25/9/20 12:12
Eliminato: overpressure ...ithin mc... [119]
Silvia 20/9/20 10:51
Eliminato: , with
Utente di Microsoft Office 23/9/20 21:28
Eliminato: minimum t compressive stress
Silvia 20/9/20 10:52
Eliminato: plot
Utente di Microsoft Office 23/9/20 21:28
Eliminato: also...orth noting impo... [120]
Utente di Microsoft Office 23/9/20 21:29
Formattato ... [121]
Silvia 25/9/20 14:31
Formattato ... [122]
Utente di Microsoft Office 25/9/20 12:12
Eliminato:
Silvia 20/9/20 10:53
Eliminato: of internal overpressure
Utente di Microsoft Office 25/9/20 12:13
Eliminato: changes ...ffects the mc... [123]
Utente di Microsoft Office 23/9/20 21:30
Eliminato: that ...eca... [124]
Silvia 20/9/20 10:54
Eliminato: . Indeed, they become
Utente di Microsoft Office 23/9/20 21:30
Eliminato: , already discussed in Figure 4

L586 mimic the effects of CR faults, describes a close to equilibrium volcanic system, in which pressure
L587 within the volcano feeding system almost equilibrate the lithostatic stress (Sulpizio et al., 2016).

L588
L589 *6.2 Some implication of the stress state of the CVC inferred from FEM*

L590 The results from the most complete FEM runs highlight an almost homogeneous stress distribution in
L591 the CVC area. This means the dual magma chamber model and the application of the far field stress
L592 provide a stable geometry, which limits the stress changes to few MPa. The majority of stress
L593 variations are located at the tips of the magma chambers, as expected for pressurized or under-
L594 pressurized cavities in the lithosphere (Martì and Geyer, 2009), implying that the whole feeding
L595 system is in a quasi-equilibrium state. Even if we consider the scenario of complete emptying the
L596 upper conduit and part of the shallow magma chamber, as occasionally occurred during the past sub-
L597 Plinian and Plinian eruptions (Lühr et al., 2002; Saucedo et al., 2010; Massaro et al., 2018), this
L598 would result in the restoration of the stress arch, which is still a stable stress configuration. Even the
L599 complete emptying of the shallow magma chamber probably would be ineffective for triggering a
L600 large collapse (caldera forming) of the feeding system.

L601 Beside and beyond the limitations due to the first order approximation of the FEM analysis, other
L602 sources of uncertainties in the discussion about present and future stress state of the CVC come from
L603 not considering gravity-driven processes, such as volcano spreading due to plastic deformation of the
L604 GF Unit (Norini et al., 2010, 2019) and detailed regional tectonics (Norini et al., 2010, 2019). The
L605 effect of the two fault systems bordering the CR are here simulated by degrading the mechanic
L606 properties of rocks in an area of about 1 km width up to a depth of 10 km. Although the effects are
L607 negligible at the scale of the computational domain, it cannot be excluded some local significant
L608 effects that cannot be resolved using the described approach.

L609
L610 **7. Summary and conclusion,**

L611 The presented study highlighted the importance to use complete and detailed geological and
L612 geophysical data when dealing with FEM of volcanic areas. The different geological detail used in

Utente di Microsoft Office 23/9/20 21:31

Eliminato: CG

Utente di Microsoft Office 25/9/20 12:20

Eliminato: volcanic

Utente di Microsoft Office 25/9/20 12:20

Eliminato: overpressure and

Utente di Microsoft Office 25/9/20 12:21

Eliminato: almost equilibrate each other

Utente di Microsoft Office 23/9/20 21:32

Eliminato: final obtained with the insertion of the full feedingfeeder

Utente di Microsoft Office 23/9/20 21:33

Eliminato: system configuration

Silvia 20/9/20 11:02

Eliminato: and far field stress on the FEM

Silvia 20/9/20 11:02

Eliminato: that the shape of

Silvia 20/9/20 11:02

Eliminato: feeding system

Silvia 20/9/20 11:02

Eliminato: and

Silvia 20/9/20 11:03

Eliminato: All the large

Silvia 20/9/20 11:03

Eliminato: . This means

Utente di Microsoft Office 23/9/20 21:34

Eliminato: , and, as an example, any overpressure created by input of new magma is adjusted by increasing the magma chamber volume or erupting at the surface

Utente di Microsoft Office 23/9/20 21:35

Eliminato: , even though .

Antonio Costa 27/9/20 12:56

Eliminato: This latter event would be possible only if a large depressurization of the deeper magma chamber would occur, but it implies the eruption of tens to hundreds of km³ of magma, which seems not very likely provided the current stress distribution in CVC.

Silvia 20/9/20 11:08

Eliminato: or pressurization of the shallower conduit (Massaro et al., 2018),

Silvia 20/9/20 11:08

Eliminato: Colima Rift

Silvia 20/9/20 11:09

Eliminato: were

Utente di Microsoft Office 25/9/20 13:51

Eliminato: Conclusi

Utente di Microsoft Office 25/9/20 13:51

Eliminato: ons

L643 the model runs showed how the stress pattern critically depends on geometry of the volcano feeding
L644 system, with huge differences in having a single or double magma chamber system and, in particular,
L645 if the magma chamber(s) are connected or not to the surface by feeder dykes and conduit. The
L646 geometry of the feeding system is prevalent on model outputs with respect to varying rock properties
L647 (i.e. Young Modulus) of one order of magnitude. In the case of CVC the use of subsurface
L648 homogeneous or stratified lithology not influence much the FEM outputs, being the subsurface
L649 geology of the computational domain dominated by carbonates (Unit B).

L650 Beside and beyond the results obtained by analysing the influence of detailed geological and
L651 geophysical data, the presented modelling confirms the close to equilibrium state of the volcano,
L652 which is the expected stress distribution induced by a feeding system directly connected to the
L653 surface.

L654 The complete emptying the upper conduit and part of the shallow magma chamber, as occasionally
L655 occurred in the past, originating sub-Plinian and Plinian eruptions, would result in the restoration of
L656 the stress arch, which is still a stable stress configuration. Descends that large magnitude, caldera
L657 forming eruptions are possible only if the bigger deep magma chamber is also involved and
L658 significantly emptied during an eruption.

L660 Appendices

L662 Appendix 1

L663 E-W gravitational modelling of the CVC domain (stratified lithology) for all configurations
L664 investigated. The magnitude and pattern of the principal stress account for a) single magma chamber
L665 model (number of nodes: 4426); b) dual magma chamber model (number of nodes: 4161); c) dual
L666 magma chamber with conduits model (number of nodes: 3737). The dimension of the deep magma
L667 chamber: $2a = 14$ km and $2b = 3.6$ km at 15 km of depth; shallow magma chamber: $2a = 3.5$ km and
L668 $2b = 2$ km at 6 km. ΔP_e and ΔP_o are equal to 20 MPa for the deep chamber, and 5 MPa for the
L669 shallower. Black dotted lines highlight the passage from different stress values. Note that the scales
L670 of stress values are different for each panel in order to maximise the simulation details.

L671

Silvia 28/9/20 10:21

Eliminato: different

Antonio Costa 27/9/20 12:58

Eliminato: Also, changing magma pressurization within the feeding system from 10 MPa to 20 MPa does not produce significant changes in stress magnitude and pattern.

Utente di Microsoft Office 25/9/20 13:43

Eliminato: The increasing details Adding detailed of geological and geophysical data to FEM simulation at Colima Volcanic Complex CVC (Mexico) showed the importance of using the most accurate input data in order to have reliable outputs. In particular, the data here presented highlighted how the use of simplified models produces unreliable outputs of the stress state of the volcano subsurface. .

Silvia 16/9/20 20:15

Eliminato: detailing

Silvia 20/9/20 11:10

Eliminato: the FEM of CVC

Silvia 16/9/20 20:17

Eliminato: This means that any overpressure created by input of new magma is adjusted within the feeding system, sometimes triggering eruptions

Utente di Microsoft Office 23/9/20 21:37

Eliminato: .

Silvia 20/9/20 11:12

Eliminato: The magmatic overpressure is

L696 **Appendix 2**

L697 E-W gravitational modelling of the CVC domain (stratified lithology) considering an [extensional](#) far-
L698 [field](#) of 5 MPa for all configurations investigated. The magnitude and pattern of the principal stress
L699 account for a) single magma chamber model (number of nodes: 4426); b) dual magma chamber
L700 model (number of nodes: 4161); c) dual magma chamber with conduits model (number of elements:
L701 3737). The dimension of the deep magma chamber: $2a = 14$ km and $2b = 3.6$ km at 15 km of depth;
L702 shallow magma chamber: $2a = 3.5$ km and $2b = 2$ km at 6 km. [ΔP_e](#) and [ΔP_ρ](#) are equal to 20 MPa for
L703 the deep chamber, and 5 MPa for the shallower. Black dotted lines highlight the passage from
L704 different stress values. The red arrows indicate the direction of the applied far field stress. Note that
L705 the [scales](#) of stress values are different for each panel in order to maximise the simulation details.

L706

L707 **Code/Data Availability**

L708 The LISA code is available at <https://lisafea.com/>.

L709

L710 **Author's contribution**

L711 SM, RS, AC, GN and GG conceived the study. SM and RS wrote the bulk of the manuscript with the
L712 input of all the co-authors. SM and GL compiled the numerical simulations and formulated the
L713 adopted methodology. MP and SM carried out the sensitivity analysis. [All the authors](#) worked on the
L714 interpretation of the results.

L715

L716 **Competing interests:** The authors declare that they have no conflict of interest.

L717 **Acknowledgements:** SM thanks the LISA customer service for the support received. [We are deeply](#)
L718 [grateful to two reviewers and the editor for the critical comments that helped us to improve the clarity](#)
L719 [and quality of the presentation.](#)

L720 **References**

L721 Albino, F., Pinel, V., and Sigmundsson, F., 2010. Influence of surface load variations on eruption
L722 likelihood: application to two Icelandic subglacial volcanoes, Grímsvötn and Katla. Geophysical
L723 journal international, 181(3), 1510-1524.
L724

Silvia 16/9/20 20:23

Eliminato: extensional stress

Silvia 28/9/20 10:23

Eliminato: model

Silvia 20/9/20 11:12

Eliminato: The magmatic overpressure

Silvia 28/9/20 10:24

Formattato: Tipo di carattere:12 pt

Silvia 28/9/20 10:24

Formattato: Tipo di carattere:14 pt

Silvia 25/9/20 14:33

Formattato: Tipo di carattere:10 pt

Silvia 28/9/20 10:24

Eliminato: is

Unknown

Codice campo modificato

Antonio Costa 27/9/20 13:00

Eliminato: RS, AC, SM, GN, GG, LC, GL, MP and AG

- [731 Albino, F., Amelung, F., and Gregg, P., 2018. The role of pore fluid pressure on the failure of magma
 [732 reservoirs: insights from Indonesian and Aleutian arc volcanoes. *Journal of Geophysical Research:*
 [733 *Solid Earth*, 123(2), 1328-1349.
- [734
 [735 Anderson E.M., 1936. The dynamics of formation of cone sheets, ring dykes and cauldron
 [736 subsidence. *Proc R Soc Edinburgh* 56:128–163.
- [737
 [738 Allan, J.F., 1985. Sediment depth in the NCG from 3-D interpretation of gravity. *Geofis. Int.* 24, 21–
 [739 30 (1985).
- [740 Allan, J.F. 1986. Geology of the Northern Colima and Zacoalco grabens, Southwest Mexico: Late
 [741 Cenozoic rifting in the Mexican Volcanic Belt. *Geol. Soc. Am. Bull.* 97, 473–485
- [742 Allan, J.F., Nelson, S.A., Luhr, J.F., Charnichael, I.S.E., Wopat, M., Wallace, P.J., 1991: Pliocene-
 [743 Holocene rifting and associated volcanism in Southwest Mexico: an exotic terrane in the making. In:
 [744 Dauphin, J.P., Simoneit, R.R.T. (eds.) *The Gulf and Peninsular Provinces of the Californias*, AAPG
 [745 Mem., vol. 47, pp. 425–445.
- [746 Andrew, R.E., and Gudmundsson, A., 2008. Volcanoes as elastic inclusions: Their effects on the
 [747 propagation of dykes, volcanic fissures, and volcanic zones in Iceland. *Journal of Volcanology and*
 [748 *Geothermal Research*, 177(4), 1045-1054.
- [749
 [750 Arámbula-Mendoza, R., Reyes-Dávila, G., Dulce, M.V.B., González-Amezcuca, M., Navarro- Ochoa,
 [751 C., Martínez-Fierros, A., and Ramírez-Vázquez, A., 2018. Seismic monitoring of effusive-explosive
 [752 activity and large lava dome collapses during 2013–2015 at Volcán de Colima, Mexico. *J. Volcanol.*
 [753 *Geotherm. Res.*, 351, 75-88.
- [754 Babuška, I., Ihlenburg, F., Paik, E. T., and Sauter, S.A., 1995. A generalized finite element method
 [755 for solving the Helmholtz equation in two dimensions with minimal pollution. *Computer methods in*
 [756 *applied mechanics and engineering*, 128(3-4), 325-359.
- [757
 [758 Bandy, W.L., Mortera-Gutiérrez, C.A., Urrutia- Fucugauchi, J., Hilde, T.W.C, 1995. The subducted
 [759 Rivera-Cocos plate boundary: where is it, what is it, and what is its relationship to the Colima Rift?
 [760 *Geophys. Res. Lett.* 22, 3075–3078.
- [761 Barrier, B., Bourgois, J., Michaud, F., 1990: The active Jalisco triple junction rift system. *C.R. Acad.*
 [762 *Sci. Paris*, 310 (II), 1513–1520.
- [763 Bathe, K. J., Zhang, H., and Ji, S., 1999. Finite element analysis of fluid flows fully coupled with
 [764 structural interactions. *Computers and Structures*, 72(1-3), 1-16.
- [765
 [766 Bonafede, M., Parenti, B., Rivalta, E., 2002. On strike-slip faulting in layered media. *Geophysical*
 [767 *Journal International*, 149(3), 698-723.
- [768
 [769 Bonasia R, Capra L, Costa A, Macedonio G, Saucedo R., 2011. Tephra fallout hazard assessment for
 [770 a Plinian eruption scenario at Volcan de Colima. *J Volcanol Geotherm Res* 203: 12–22.
- [771
 [772 Boresi, A.P., Schmidt, R.J., and Sidebottom, O.M., 1985. *Advanced mechanics of materials* (Vol. 6).
 [773 New York et al.: Wiley.
- [774
 [775 Buchmann T. and Conolly P.T., 2007. Contemporary kinematics of the Upper Rhine Graben: A 3D
 [776 finite element approach. *Global and Planetary Change* 58, 287–309.
- [777
 [778 Bunnay, 2014. *The Effects of Structural Heterogeneities and In-elastic Rheology on Ground
 Deformation at Campi Flegrei Caldera, Italy.* PhD Thesis.
- [779 Cabaniss, H.E., Gregg, P. M., and Grosfils, E.B., 2018. The role of tectonic stress in triggering large
 [780 silicic caldera eruptions. *Geophysical Research Letters*, 45, 3889–3895. <https://doi.org/10.1029/>

1781 2018GL077393.

1782 Cayol, V., and Cornet, F. H., 1998. Effects of topography on the interpretation of the deformation
1783 field of prominent volcanoes: Application to Etna. *Geophysical Research Letters*, 25(11), 1979–1982.
1784 <https://doi.org/10.1029/98GL51512>.

1785
1786 Cailleau, B., T.R. Walter, P. Janle, and E. Hauber, 2003. Modeling volcanic deformation in a regional
1787 stress field: Implications for the formation of graben structures on Alba Patera, Mars, *J. Geophys.*
1788 *Res.*, 108(E12), 5141, doi:10.1029/2003JE002135.

1789 Cailleau B., Thomas R. Walter, Peter Janle, Ernst Hauber, 2005. Unveiling the origin of radial
1790 grabens on Alba Patera volcano by finite element modelling *Icarus* 176, 44–56.

1791
1792 Cabrera-Gutiérrez, R., and Espíndola, J.M., 2010. The 1998-1999 eruption of Volcán de Colima,
1793 Mexico: an application of Maeda's viscoelastic model. *Geofísica internacional*, 49(2), 83-96.

1794
1795 Canales, J.P., Nedimović, M.R., Kent, G.M., Carbotte, S.M., and Detrick, R.S., 2009. Seismic
1796 reflection images of a near-axis melt sill within the lower crust at the Juan de Fuca ridge. *Nature*,
1797 460(7251), 89.

1798
1799 Capra, L., and Macías, J.L., 2002. The cohesive Naranjo debris-flow deposit (10 km³): A dam
1800 breakout flow derived from the Pleistocene debris-avalanche deposit of Nevado de Colima Volcano
1801 (México). *Journal of Volcanology and Geothermal Research*, 117(1-2), 213-235.

1802
1803 Capra L, Macías JL, Cortés A, Dávila N, Saucedo R, Osorio-Ocampo S, Arce JL, Galvilanes-Ruiz JC,
1804 Corona-Càvez P, Gàrcia-Sanchez L, Sosa-Ceballos G, Vasquez R., 2016. Preliminary report on the
1805 July 10–11, 2015 eruption at Volcán de Colima: Pyroclastic density currents with exceptional runouts
1806 and volume, *J Volcanol Geotherm Res* 310: 39-49.

1807
1808 Cianetti, S., Giunchi, C., and Casarotti, E., 2012. Volcanic deformation and flank instability due to
1809 magmatic sources and frictional rheology: the case of Mount Etna. *Geophysical Journal International*,
1810 191(3), 939-953.

1811
1812 Charco, M., and Galán del Sastre, P., 2014. Efficient inversion of three-dimensional finite element
1813 models of volcano deformation. *Geophysical Journal International*, 196(3), 1441-1454.

1814
1815 Chaput, M., Pinel, V., Famin, V., Michon, L., and Froger, J.L., 2014. Cointrusive shear displacement
1816 by sill intrusion in a detachment: A numerical approach. *Geophysical Research Letters*, 41(6), 1937-
1817 1943.

1818
1819 Cortés, A., 2005. Carta geológica del complejo volcánico de Colima. UNAM, Instituto de Geología.

1820
1821 Cortés, A., Garduño, V.H., Macías, J. L., Navarro-Ochoa, C., Komorowski, J.C., Saucedo, R., and
1822 Gavilanes, J. C. (2010). Geologic mapping of the Colima volcanic complex (Mexico) and
1823 implications for hazard assessment. *Geol Soc Am Spec Pap*, 464, 249-264.

1824
1825 Cortés, A., Komorowski, J. C., Macías, J. L., Capra, L., and Layer, P. W., 2019. Late Pleistocene-
1826 Holocene debris avalanche deposits from Volcán de Colima, Mexico. In *Volcán de Colima* (pp. 55-
1827 79). Springer, Berlin, Heidelberg.

1828
1829 Costa, A., Sparks, R.S.J., Macedonio, G., and Melnik, O., 2009. Effects of wall-rock elasticity on
1830 magma flow in dykes during explosive eruptions. *Earth and Planetary Science Letters*, 288(3-4), 455-
1831 462.

1832
1833 Costa, A., Gottsmann, J., Melnik, O., and Sparks, R. S. J., 2011. A stress-controlled mechanism for
1834 the intensity of very large magnitude explosive eruptions. *Earth and Planetary Science Letters*, 310(1-
1835 2), 161-166.

1836

Unknown

Codice campo modificato

Utente di Microsoft Office 22/9/20 11:10

Formattato: Italiano

Utente di Microsoft Office 22/9/20 11:10

Formattato: Italiano

Utente di Microsoft Office 22/9/20 11:10

Formattato: Italiano

- ‡837 Currenti, G., Bonaccorso, A., Del Negro, C., Scandura, D., and Boschi, E., 2010. Elasto-plastic
‡838 modeling of volcano ground deformation. *Earth and Planetary Science Letters*, 296(3-4), 311-318.
‡839
- ‡840 Currenti, G., and Williams, C.A., 2014. Numerical modeling of deformation and stress fields around
‡841 a magma chamber: Constraints on failure conditions and rheology. *Physics of the Earth and Planetary
‡842 Interiors*, 226, 14-27.
‡843
- ‡844 Dávila, N., Capra, L., Ferrés, D., Gavilanes-Ruiz, J. C., and Flores, P., 2019. Chronology of the
‡845 2014–2016 Eruptive Phase of Volcán de Colima and Volume Estimation of Associated Lava Flows
‡846 and Pyroclastic Flows Based on Optical Multi-Sensors. *Remote Sensing*, 11(10), 1167.
‡847
- ‡848 Del Potro, R. and Hürlimann, M., 2008. Geotechnical classification and characterization of materials
‡849 for stability analyses of large volcanic slopes. *Eng. Geol.* 98(1), 1–17.
- ‡850 Dieterich J.H., and R.W. Decker, 1975. Finite element modeling of surface deformation associated
‡851 with volcanism, *J. Geophys. Res.*, 80, 4094–4102.
- ‡852 Escudero, C.R., and Bandy, W.L., 2017: Ambient seismic noise tomography of the Colima Volcano
‡853 Complex. *Bull. Volcanol.* 79, 13.
- ‡854 Fernández, J., Tiampo, K. F., Jentzsch, G., Charco, M., and Rundle, J.B., 2001. Inflation or deflation?
‡855 New results for Mayon Volcano applying elastic - gravitational modeling. *Geophysical Research
‡856 Letters*, 28(12), 2349-2352.
‡857
- ‡858 Ferrari, L., Rosas-Elguera, J., Márquez, A., Oyarzun, R., Doblás, M., and Verma, S.P., 1999. Alkalic
‡859 (ocean-island basalt type) and calc-alkalic volcanism in the Mexican volcanic belt: A case for plume-
‡860 related magmatism and propagating rifting at an active margin?: Comment and Reply. *Geology*,
‡861 27(11), 1055-1056.
‡862
- ‡863 Folch, A., Fernández, J., Rundle, J.B., Martí, J., 2000. Ground deformation in a viscoelastic medium
‡864 composed of a layer overlying a half-space: a comparison between point and extended sources.
‡865 *Geophys. J. Int.* 140 (1), 37–50.
- ‡866 Frey, H.M., Lange, R.A., Hall, C.M., Delgado-Granados, H., Carmichael, I.S.E., 2007. A Pliocene
‡867 ignimbrite flare-up along the Tepic-Zacoalco rift: evidence for the initial stages of rifting between the
‡868 Jalisco block (Mexico) and North America. *Geol. Soc. Am. Bull.* 119, 49–64.
‡869 <http://dx.doi.org/10.1130/B25950.1>.
- ‡870 Fujita, E., Kozono, T., Ueda, H., Kohno, Y., Yoshioka, S., Toda, N., and Ida, Y., 2013. Stress field
‡871 change around the Mount Fuji volcano magma system caused by the Tohoku megathrust earthquake,
‡872 Japan. *Bulletin of volcanology*, 75(1), 679.
‡873
- ‡874 Gabrieli, A., Wilson, L., and Lane, S., 2015. Volcano–tectonic interactions as triggers of volcanic
‡875 eruptions. *Proceedings of the Geologists' Association*, 126(6), 675-682.
‡876
- ‡877 Garduño-Monroy, V.H., Saucedo-Girón, R., Jiménez, Z., Gavilanes-Ruiz, J.C., Cortés-Cortés, A.,
‡878 Uribe-Cifuentes, R.M. 1998: La Falla Tamazula, límite suroriental del Bloque Jalisco, y sus
‡879 relaciones con el Complejo Volcánico de Colima, México. *Revista Mexicana de Ciencias Geológicas*
‡880 15(2), 132–144.
- ‡881 Gelman, S.E., Deering, C.D., Gutierrez, F.J., and Bachmann, O., 2013. Evolution of the Taupo
‡882 Volcanic Center, New Zealand: petrological and thermal constraints from the Omega dacite.
‡883 *Contributions to Mineralogy and Petrology*, 166(5), 1355-1374.
‡884
- ‡885 Geyer, A., and Martí, J., 2009. Stress fields controlling the formation of nested and overlapping
‡886 calderas: implications for the understanding of caldera unrest. *Journal of Volcanology and
‡887 Geothermal Research*, 181(3-4), 185-195.
‡888
- ‡889 Geyer, A., and Gottsmann, J., 2010. The influence of mechanical stiffness on caldera deformation

- and implications for the 1971–1984 Rabaul uplift (Papua New Guinea). *Tectonophysics*, 483(3-4), 399-412.
- Geyer, A., Martí, J., and Villaseñor, A., 2016. First-order estimate of the Canary Islands plate-scale stress field: Implications for volcanic hazard assessment. *Tectonophysics*, 679, 125-139.
- Gerbault, M., Cappa, F., Hassani, R., 2012. Elasto-plastic and hydromechanical models of failure around an infinitely long magma chamber. *Geochem. Geophys. Geosyst.* 13, Q03009. <http://dx.doi.org/10.1029/2011GC003917>.
- Gerbault, M., Hassani, R., Lizama CN, Souche, A., 2018. Three-Dimensional Failure Patterns Around an Inflating Magmatic Chamber. *Geochemistry, Geophysics, Geosystems*, AGU and the Geochemical Society, In press.
- Geshi, N., Kusumoto, S., and Gudmundsson, A., 2012. Effects of mechanical layering of host rocks on dike growth and arrest. *Journal of Volcanology and Geothermal Research*, 223, 74-82.
- Grosfils, E.B., 2007. Magma reservoir failure on the terrestrial planets: Assessing the importance of gravitational loading in simple elastic models, *J. Volcanol. Geotherm. Res.*, 166, 47–75, doi:10.1016/j.jvolgeores.2007.06.007.
- Grosfils, E.B., McGovern, P. J., Gregg, P.M., Galgana, G.A., Hurwitz, D.M., Long, S.M., Chestler, S.R., 2015. Elastic models of magma reservoir mechanics: a key tool for investigating planetary volcanism. *Geol. Soc. London, Spec. Pub.*, 401(1), 239-267.
- Gudmundsson, A., and Brenner, S.L., 2004. How mechanical layering affects local stresses, unrests, and eruptions of volcanoes. *Geophysical Research Letters*, 31(16).
- Gudmundsson, A., 2006. How local stresses control magma-chamber ruptures, dyke injections, and eruptions in composite volcanoes, *Earth-Sci.Rev.*, 79(1–2), 1–31.
- Gudmundsson, A., 2011. *Rock fractures in geological processes*. Cambridge University Press.
- [Gudmundsson, A. \(2012\). Magma chambers: Formation, local stresses, excess pressures, and compartments. *Journal of Volcanology and Geothermal Research*, 237, 19-41.](#)
- Goennermann and Taisne, 2015. Magma Transport in Dikes. *The Encyclopedia of Volcanoes*. <http://dx.doi.org/10.1016/B978-0-12-385938-9.00010-9>.
- Gottsmann, J., Folch, A., and Rymer, H., 2006. Unrest at Campi Flegrei: A contribution to the magmatic versus hydrothermal debate from inverse and finite element modeling. *Journal of Geophysical Research: Solid Earth*, 111(B7).
- Gutiérrez, F., and Parada, M.A., 2010. Numerical modeling of time-dependent fluid dynamics and differentiation of a shallow basaltic magma chamber. *Journal of Petrology*, 51(3), 731-762.
- Hautmann, S., Gottsmann, J., Sparks, R.S.J., Costa, A., Melnik, O., and Voight, B., 2009. Modelling ground deformation caused by oscillating overpressure in a dyke conduit at Soufrière Hills Volcano, Montserrat. *Tectonophysics*, 471(1-2), 87-95.
- Heap, M. J., Villeneuve, M., Albino, F., Farquharson, J. I., Brothelande, E., Amelung, F., and Baud, P., 2020. Towards more realistic values of elastic moduli for volcano modelling. *Journal of Volcanology and Geothermal Research*, 390, 106684.
- Hickey, J., Gottsmann, J., and Mothes, P., 2015. Estimating volcanic deformation source parameters with a finite element inversion: The 2001–2002 unrest at Cotopaxi volcano, Ecuador, *J. Geophys. Res. Solid Earth*, 120, 1473–1486, doi:10.1002/2014JB011731.

Silvia 28/9/20 10:17

Formattato: Tipo di carattere:(Predefinito) Times, 12 pt, (Asian) Giapponese, (Other) Inglese (Regno Unito)

Silvia 28/9/20 10:17

Formattato: Tipo di carattere:(Predefinito) Times, 12 pt, Non Corsivo, (Asian) Giapponese, (Other) Inglese (Regno Unito)

Silvia 28/9/20 10:17

Formattato: Tipo di carattere:(Predefinito) Times, 12 pt, (Asian) Giapponese, (Other) Inglese (Regno Unito)

- 1941 Hoek, E. and Brown, E.T., 1997. Practical estimates of rock mass strength. *Int. J. Rock Mech. Min. Sci.* 34, 1165–1186.
 1942
- 1943 Holohan, E.P., Schöpfer, M. P. J., and Walsh, J.J., 2015. Stress evolution during caldera collapse. *Earth and Planetary Science Letters*, 421, 139-151.
 1944
- 1945 Huang, X., and Zhang, Z., 2012. Stress arch bunch and its formation mechanism in blocky stratified rock masses. *Journal of Rock Mechanics and Geotechnical Engineering*, 4(1), 19-27.
 1946
 1947
- 1948 Karlstrom, L., Dufek, J., Manga, M., 2010. Magma chamber stability in arc and continental crust. *J. Volcanol. Geotherm. Res.* 190, 249–270.
 1949
 1950
- 1951 Kinvig, H. S., Geyer, A., and Gottsmann, J., 2009. On the effect of crustal layering on ring-fault initiation and the formation of collapse calderas. *Journal of Volcanology and Geothermal Research*, 186(3-4), 293-304.
 1952
 1953
- 1954 Jaeger, J.C., Cook, N.G., and Zimmerman, R., 2009. *Fundamentals of rock mechanics*. John Wiley and Sons.
 1955
 1956
- 1957 Jeanne, P., Guglielmi, Y., Rutqvist, J., Nussbaum, C., and Birkholzer, J., 2017. Field characterization of elastic properties across a fault zone reactivated by fluid injection. *Journal of Geophysical Research: Solid Earth*, 122(8), 6583-6598.
 1958
 1959
- 1960 Jellinek, A.M. and DePaolo, D.J., 2003. A model for the origin of large silicic magma chambers: precursors of caldera-forming eruptions. *Bull. Volcanol.* 65, 363–381.
 1961
 1962
- 1963 Lister, J.R. and Kerr, R.C., 1991. Fluid-mechanical models of crack propagation and their application to magma transport in dykes. *Journal of Geophysical Research* 96,10,049–10,077.
 1964
 1965
- 1966 Long, S.M., and Grosfils, E.B., 2009. Modeling the effect of layered volcanic material on magma reservoir failure and associated deformation, with application to Long Valley caldera, California. *Journal of Volcanology and Geothermal Research*, 186(3-4), 349-360.
 1967
 1968
- 1969 López-Loera, H., Urrutia-Fucugauchi, J., Alva-Valdivia, L., 2011. Estudio aeromagnético del complejo volcánico de Colima, occidente de México – implicaciones tectónicas y estructurales. *Revista Mexicana de Ciencias Geológicas* 28, 349–370.
 1970
 1971
- 1972 Lungarini, L., Troise, C., Meo, M., and De Natale, G., 2005. Finite element modelling of topographic effects on elastic ground deformation at Mt. Etna. *Journal of volcanology and geothermal research*, 144(1-4), 257-271.
 1973
 1974
- 1975 Luhr, J.F., and Carmichael, I.S., 1985. Contemporaneous eruptions of calc-alkaline and alkaline magmas along the volcanic front of the Mexican Volcanic Belt. *Geofísica Internacional*, 24(1).
 1976
 1977
- 1978 Luhr, J.F., and Prestegard, K.L., 1988. Caldera formation at Volcán Colima, Mexico, by a large holocene volcanic debris avalanche. *Journal of Volcanology and Geothermal Research*, 35(4), 335-348.
 1979
 1980
- 1981 Luhr JF., 2002. Petrology and geochemistry of the 1991 and 1998-1999 lava flows from Volcan Colima, Mexico. *J Volcanol Geotherm Res* 117: 169–194.
 1982
 1983
 1984
- 1985 Maccaferri, F., Bonafede, M., and Rivalta, E., 2010. A numerical model of dyke propagation in layered elastic media. *Geophysical Journal International*, 180(3), 1107-1123.
 1986
 1987
- 1988 Maccaferri, F., Bonafede, M., and Rivalta, E., 2011. A quantitative study of the mechanisms governing dike propagation, dike arrest and sill formation. *Journal of Volcanology and Geothermal Research*, 208(1-2), 39-50.
 1989
 1990
 1991
 1992
 1993

- 1994 Maccaferri, F., Rivalta, E., Keir, D., and Acocella, V., 2014. Off-rift volcanism in rift zones
 1995 determined by crustal unloading. *Nature Geoscience*, 7(4), 297-300.
 1996
 1997 Maccaferri, F., Smittarello, D., Pinel, V., and Cayol, V., 2019. On the propagation path of magma-
 1998 filled dikes and hydrofractures: The competition between external stress, internal pressure, and crack
 1999 length. *Geochemistry, Geophysics, Geosystems*, 20(4), 2064-2081.
 2000
 2001 Macías, J.L., Saucedo, R., Gavilanes, J.C., Varley, N., Velasco, García S., Bursik, M.I., Vargas,
 2002 Gutiérrez V., Cortés, A., 2006. Flujos piroclásticos asociados a la activi- dad explosiva del Volcán de
 2003 Colima y perspectivas futuras. *GEOS* 25(3), 340–351.
- 2004 Macias J, Arce J, Sosa G, Gardner JE, Saucedo R., 2017. Storage conditions and magma processes
 2005 triggering the 1818CE Plinian eruption of Volcán de Colima. *J Volcanol GeothermRes*
 2006 doi:10.1016/j.jvolgeores.2017.02.025.
- 2007 Macdonald, K.C., 1982. Mid-ocean ridges: fine scale tectonic, volcanic and hydrothermal pro-
 2008 cesses within the plate boundary zone. *Annual Review of Earth and Planetary Sciences* 10, 155–190.
- 2009 MacLeod, C.J., Yaouancq, G., 2000. A fossil melt lens in the Oman ophiolite: implications for
 2010 magma chamber processes at fast spreading ridges. *Earth and Planetary Science Letters* 176, 357–373.
- 2011 Manconi A., Walter TR, and Amelung, F., 2007. Effects of mechanical layering on volcano
 2012 deformation. *Geophys. J. Int.* (2007) 170, 952–958.
- 2013 Manconi, A., Longpré, M.A., Walter, T.R., Troll, V.R., Hansteen, T.H., 2009. The effects of flank
 2014 collapses on volcano plumbing systems. *Geology* 37 (12), 1099–1102.
- 2015 Marinou, P. and Hoek, E., 2000. GSI: a geologically friendly tool for rock mass strength estimation.
 2016 In: *Proc. GeoEng2000 Conference*, Melbourne, 1422–1442.
- 2017 Martí, J., and Geyer, A., 2009. Central vs flank eruptions at Teide–Pico Viejo twin stratovolcanoes
 2018 (Tenerife, Canary Islands). *Journal of Volcanology and Geothermal Research*, 181(1-2), 47-60.
 2019
- 2020 Massaro S, Sulpizio R, Costa A, Capra L., Lucchi F., 2018. Understanding eruptive style variations at
 2021 calc-alkaline volcanoes: the 1913 eruption of Fuego de Colima volcano (Mexico). *Bulletin of*
 2022 *Volcanology*, 80:62.
- 2023 Massaro, S., Costa, A., Sulpizio, R., Coppola, D., Capra, L., 2019. Cyclic activity of Fuego de
 2024 Colima volcano (Mexico): insights from satellite thermal data and non-linear models. *Solid Earth*,
 2025 1429-1450.
- 2026 Margottini, C., Canuti, P., Sassa, K., 2013. *Landslide science and practice (Vol. 1)*. Berlin: Springer.
- 2027
 2028 Masterlark, T., Feigl, K.L., Haney, M., Stone, J., Thurber, C., and Ronchin, E., 2012. Nonlinear
 2029 estimation of geometric parameters in FEMs of volcano deformation: Integrating tomography models
 2030 and geodetic data for Okmok volcano, Alaska. *Journal of Geophysical Research: Solid Earth*,
 2031 117(B2).
 2032
- 2033 Medina-Martínez, F., Espíndola, J.M., De la Fuente, M., Mena, M., 1996. A gravity model of the
 2034 Colima, México region. *Geofis. Int.* 35(4), 409–414.
- 2035 Michaeli, W., 1991. *Extrusionswerkzeuge für Kunststoffe und Kautschuk: Bauarten, Gestaltung und*
 2036 *Berechnungsmöglichkeiten*. Hanser Verlag.
- 2037
 2038 Moeck, I., Schandelmeier, H. and Holl, H.G., 2009. The stress regime in a Rotliegend reservoir of
 2039 the Northeast German Basin. *Int. J. Earth. Sci.* 98, 1643-1654.
- 2040 Mutter, J.C., Carbotte, S.M., Su, W.S., Xu, L.Q., Buhl, P., Detrick, R.S., Kent, G.M., Orcutt, J.A.,
 2041 Harding, A.J., 1995. Seismic images of active magma systems beneath the East Pacific Rise between

Unknown

Codice campo modificato

2042 17-degrees-05's and 17-degrees-35's. *Science* 268, 391–395.
 2043 Newman, A. V., Dixon, T. H., Ofoegbu, G. I., and Dixon, J. E., 2001. Geodetic and seismic
 2044 constraints on recent activity at Long Valley Caldera, California: evidence for viscoelastic rheology.
 2045 *Journal of Volcanology and Geothermal Research*, 105(3), 183-206.
 2046
 2047 Norini, G., Agliardi, F., Crosta, G., Groppelli, G., and Zuluaga, M.C., 2019. Structure of the Colima
 2048 Volcanic Complex: Origin and Behaviour of Active Fault Systems in the Edifice. In *Volcán de*
 2049 *Colima* (pp. 27-54). Springer, Berlin, Heidelberg.
 2050
 2051 Norini G, Capra L, Groppelli G, Agliardi F, Pola A, Cortes A., 2010. Structural architecture of the
 2052 Colima Volcanic Complex. *J Geophys Res* 115, B12209.
 2053
 2054 Núñez-Cornú F, Nava FA, De la Cruz-Reyna S, Jiménez Z, Valencia C, García-Arthur R., 1994.
 2055 Seismic activity related to the 1991 eruption of Colima Volcano, Mexico. *Bull Volcanol* 56: 228–237.
 2056
 2057 Parfitt, E. A., and L. Wilson, 2008. "The role of volatiles." *Fundamentals of Physical Volcanology*,
 2058 64-76.
 2059
 2060 Pinel, V., and Jaupart, C., 2004. Magma storage and horizontal dyke injection beneath a volcanic
 2061 edifice. *Earth and Planetary Science Letters*, 221(1-4), 245-262.
 2062
 2063 Pinel, V., Carrara, A., Maccaferri, F., Rivalta, E., and Corbi, F., 2017. A two-step model for
 2064 dynamical dike propagation in two dimensions: Application to the July 2001 Etna eruption. *Journal*
 2065 *of Geophysical Research: Solid Earth*, 122(2), 1107-1125.
 2066
 2067 Pritchard, M. E., and Simons, M., 2004. An InSAR-based survey of volcanic deformation in the
 2068 central Andes. *Geochemistry, Geophysics, Geosystems*, 5(2).
 2069
 2070 Rao S.S., 1989. *The Finite Element Method in Engineering* second edition. PERGAMON PRESS
 2071 1989 ISBN 0-08-033419-9.
 2072
 2073 Rao, S.S., 2013. *The Finite Element Method in Engineering: Pergamon International Library of*
 2074 *Science, Technology, Engineering and Social Studies*. Elsevier.
 2075
 2076 Reubi, O., Blundy, J., and Varley, N.R., 2013. Volatiles contents, degassing and crystallisation of
 2077 intermediate magmas at Volcan de Colima, Mexico, inferred from melt inclusions. *Contributions to*
 2078 *Mineralogy and Petrology*, 165(6), 1087-1106.
 2079
 2080 Reubi, O., Blundy, J., and Pickles, J., 2019. Petrological monitoring of Volcán de Colima magmatic
 2081 system: the 1998 to 2011 activity. In *Volcán de Colima* (pp. 219-240). Springer, Berlin, Heidelberg.
 2082 Rivalta et al., 2019. Stress inversions to forecast magma pathways and eruptive vent location *Sci*.
 Adv. 2019; 5:eaa9784 .
 2083
 2084 Rivalta, E., Corbi, F., Passarelli, L., Acocella, V., Davis, T., and Di Vito, M.A., 2019. Stress
 2085 inversions to forecast magma pathways and eruptive vent location. *Science advances*, 5(7), eaa9784.
 2086
 2087 Robin, C., Mossand, P., Camus, G., Cantagrel, J. M., Gourgaud, A., and Vincent, P.M., 1987.
 2088 Eruptive history of the Colima volcanic complex (Mexico). *Journal of Volcanology and Geothermal*
 2089 *Research*, 31(1-2), 99-113.
 2090
 2091 Ronchin, E., Masterlark, T., Molist, J. M., Saunders, S., and Tao, W., 2013. Solid modeling
 2092 techniques to build 3D finite element models of volcanic systems: an example from the Rabaul
 2093 Caldera system, Papua New Guinea. *Computers & Geosciences*, 52, 325-333.
 2094
 2095 Ronchin, E., Geyer, A., and Martí, J., 2015. Evaluating topographic effects on ground deformation:
 2096 insights from finite element modeling. *Surveys in Geophysics*, 36(4), 513-548.
 2097
 2098 Rosas-Elguera, J., Ferrari, L., Garduño-Monroy, V.H., Urrutia-Fucugauchi, J., 1996: *Continental*

- ?098 boundaries of the Jalisco block and their influence in the Pliocene-Quaternary kinematics of western
 ?099 Mexico. *Geology* 24, 921–924.
- ?100 Rosas-Elguera J, Ferrari L, Martínez ML, Urrutia-Fucugauchi J., 1997. Stratigraphy and tectonics of
 ?101 the Guadalajara region and triple- junction area, western Mexico. *Int Geol Rev* 39:125–140.
 ?102 doi:10.1080/00206819709465263.
- ?103 Rosas-Elguera, J., Alva-Valdivia, L. M., Goguitchaichvili, A., Urrutia-Fucugauchi, J., Ortega-Rivera,
 ?104 M. A., Prieto, J.C.S., and Lee, J.K., 2003. Counterclockwise rotation of the Michoacan Block:
 ?105 implications for the tectonics of western Mexico. *International Geology Review*, 45(9), 814-826.
 ?106
- ?107 Roverato, M., Capra, L., Sulpizio, R., Norini, G., 2011. Stratigraphic reconstruction of two debris
 ?108 avalanche deposits at Colima Volcano (Mexico): insights into pre-failure conditions and climate
 ?109 influence. *Journal of Volcanology and Geothermal Research*, 207(1-2), 33-46, 2011
- ?110 Roverato, M., and Capra, L., 2013. Características microtexturales como indicadores del transporte y
 ?111 emplazamiento de dos depósitos de avalancha de escombros del Volcán de Colima (México). *Revista
 ?112 mexicana de ciencias geológicas*, 30(3), 512-525.
 ?113
- ?114 Salzer J.T., Nikkhoo M., Walter T., Sudhaus H., Reyes-Dávila G., Bretón-Gonzalez M., Arámbula R.,
 ?115 2014. Satellite radar data reveal short-term pre-explosive displacements and a complex conduit
 ?116 system at Volcan de Colima, Mexico. *Front Earth Sci* 2:12.
 ?117
- ?118 Saada, A.S., 2009. *Elasticity: Theory and Applications*. Krieger, Malabar, Florida.
- ?119 Savin, G. N., 1961. Stress concentration around holes.
 ?120
- ?121 Saucedo R, Macías J., Gavilanes JC, Arce JL, Komorowski JC, Gardner JE, Valdez-Moreno G., 2010.
 ?122 Eyewitness, stratigraphy, chemistry, and eruptive dynamics of the 1913 Plinian eruption of Volcán
 ?123 de Colima. México. *J Volcanol Geotherm Res* 191:149–166.
 ?124
- ?125 Saucedo R, Macías JL, Gavilanes JC, Arce JL, Komorowski JC, Gardner JE, and Valdez-Moreno G.,
 ?126 2011. Corrigendum to Eyewitness, stratigraphy, chemistry, and eruptive dynamics of the 1913 plinian
 ?127 eruption of Volcan de Colima, Mexico. *J Volcanol Geotherm Res* 191:149–166.
 ?128
- ?129 Schwarz, H.R., 1991. *Methode der finiten Elemente neubearbeitete Auflage*, B.G. Teubner Stuttgart
 ?130 ISBN 3-519-22349-X.
- ?131 Selvans, M. M., Stock, J. M., DeMets, C., Sanchez, O., and Marquez-Azua, B., 2011. Constraints on
 ?132 Jalisco Block motion and tectonics of the Guadalajara triple junction from 1998–2001 Campaign
 ?133 GPS Data. *Pure and applied geophysics*, 168(8-9), 1435-1447.
 ?134
- ?135 Serpa, L., Smith, S., Katz, C., Skidmore, C., Sloan, R., Pavlis, T., 1992. A geophysical investigation
 ?136 of the southern Jalisco block in the state of Colima, Mexico. *Geofísica Internacional* 31, 247–252.
- ?137 Simms MA., and Graven G., 2004. Thermal convection in faulted extensional sedimentary basins:
 ?138 theoretical results from finite-element modelling. *Geofluids* (2004), 4, 109-130.
 ?139
- ?140 Singh, S. C., Crawford, W. C., Carton, H., Seher, T., Combier, V., Cannat, M., and Miranda, J. M.,
 ?141 2006. Discovery of a magma chamber and faults beneath a Mid-Atlantic Ridge hydrothermal field.
 ?142 *Nature*, 442(7106), 1029.
 ?143
- ?144 Sinton, J.M., and Detrick, R.S., 1992. Mid-ocean ridge magma chambers. *Journal of Geophysical
 ?145 Research: Solid Earth*, 97(B1), 197-216.
 ?146
- ?147 Stock JM and Lee J., 1994. Do microplates in subduction zones leave a geological record? *Tectonics*
 ?148 13:1472–1487.

?149 Stoopes, G. R., and Sheridan, M.F., 1992. Giant debris avalanches from the Colima Volcanic
 ?150 Complex, Mexico: Implications for long-runout landslides (> 100 km) and hazard assessment.
 ?151 *Geology*, 20(4), 299-302.
 ?152
 ?153 Spica, Z., Cruz-Atienza, V.M., Reyes-Alfaro, G., Legrand, D., and Iglesias, A., 2014. Crustal
 ?154 imaging of western Michoacán and the Jalisco Block, Mexico, from ambient seismic noise. *Journal*
 ?155 *of Volcanology and Geothermal Research*, 289, 193-201.
 ?156
 ?157 Spica Z, Perton M, Legrand D., 2017. Anatomy of the Colima volcano magmatic system,
 ?158 Mexico, *Earth Planet Sci Lett* 459: 1-13.
 ?159
 ?160 Suárez, G., Garcia-Acosta, V., Gaulon, R., 1994. Active crustal deformation in the Jalisco block,
 ?161 Mexico: evidence for a great historical earthquake in the 16th century. *Tectonophysics* 234, 117–12.
 ?162
 ?163 Sulpizio, R., Lucchi, F., Forni, F., Massaro, S., and Tranne, C., 2016. Unravelling the effusive-
 ?164 explosive transitions and the construction of a volcanic cone from geological data: The example of
 ?165 Monte dei Porri, Salina Island (Italy). *Journal of Volcanology and Geothermal Research*, 327, 1-22.
 ?166
 ?167 Sulpizio, R., and Massaro, S., 2017. Influence of stress field changes on eruption initiation and
 ?168 dynamics: a review. *Frontiers in Earth Science*, 5, 18.
 ?169
 ?170 Tibaldi, A., 2015. Structure of volcano plumbing systems: A review of multi-parametric effects.
 ?171 *Journal of Volcanology and Geothermal Research* 298 (2015) 85–135.
 ?172
 ?173 Touloukian, Y.S., Judd, W.R., Roy, R.F., 1989. *Physical Properties of Rocks and Minerals*, vol. 548.
 ?174 Hemisphere, New York.
 ?175
 ?176 Turcotte, D. L. and Schubert, G., 2002. *Geodynamics*, 2nd edition, Cambridge University Press.
 ?177
 ?178 Zehner B, Jana H. Börner J.H., Görz I., Spitzer K., 2015. Workflows for generating tetrahedral
 ?179 meshes for finite element simulations on complex geological structures. *Computers and Geosciences*,
 ?180 79, 105-117.
 ?181
 ?182 Zhao, S., Muller, R. D., Takahashi, Y. and Kaneda, Y., 2004. 3-D finite-element modelling of
 ?183 deformation and stress associated with faulting: effect of inhomogeneous crustal structures, *Geophys.*
 ?184 *J. Int.*, 157, 629– 644.
 ?185
 ?186 Zhong, X. Marcin, Dabrowski, Bjørn Jamtveit, 2019. Analytical solution for the stress field in elastic
 ?187 half space with a spherical pressurized cavity or inclusion containing eigenstrain. *Geophysical*
 ?188 *Journal International* · (submitted).
 ?189
 ?190 Zobin, V.M., Luhr, J.F., Taran, Y.A., Bretón, M., Cortés, A., De la Cruz-Reyna, S., Domínguez, T.,
 ?191 Galindo, I., Gavilanes, J.C., Muñoz, J.J., Navarro, C., Ramírez, J. J., Reyes, G.A., Ursúa, M., Velasco,
 ?192 J., Alatorre, E., Santiago, H., 2002. Overview of the 1997–2000 activity of Volcán de Colima,
 ?193 Mexico. *J. Volcanol. Geotherm. Res.* 117, 1–19.
 ?194
 ?195 Watanabe, T., Masuyama, T., Nagaoka, K., Tahara, T., 2002. Analog experiments on magma-filled
 ?196 cracks: competition between external stresses and internal pressure. *Earth Planets Space* 54, 1247–
 ?197 1261.
 ?198
 ?199 Wang, R., Martin, F.L. and Roth, F., 2003. Computation of deformation induced by earthquakes in a
 ?200 multi-layered elastic crust-FORTRAN programs EDGRN/EDCMP, *Comput. Geosci.*, 29, 195–207.
 ?201
 ?202
 ?203
 ?204
 ?205
 ?206
 ?207
 ?208
 ?209
 ?210
 ?211
 ?212
 ?213
 ?214
 ?215
 ?216
 ?217
 ?218
 ?219
 ?220
 ?221
 ?222
 ?223
 ?224
 ?225
 ?226
 ?227
 ?228
 ?229
 ?230
 ?231
 ?232
 ?233
 ?234
 ?235
 ?236
 ?237
 ?238
 ?239
 ?240
 ?241
 ?242
 ?243
 ?244
 ?245
 ?246
 ?247
 ?248
 ?249
 ?250
 ?251
 ?252
 ?253
 ?254
 ?255
 ?256
 ?257
 ?258
 ?259
 ?260
 ?261
 ?262
 ?263
 ?264
 ?265
 ?266
 ?267
 ?268
 ?269
 ?270
 ?271
 ?272
 ?273
 ?274
 ?275
 ?276
 ?277
 ?278
 ?279
 ?280
 ?281
 ?282
 ?283
 ?284
 ?285
 ?286
 ?287
 ?288
 ?289
 ?290
 ?291
 ?292
 ?293
 ?294
 ?295
 ?296
 ?297
 ?298
 ?299
 ?300
 ?301
 ?302
 ?303
 ?304
 ?305
 ?306
 ?307
 ?308
 ?309
 ?310
 ?311
 ?312
 ?313
 ?314
 ?315
 ?316
 ?317
 ?318
 ?319
 ?320
 ?321
 ?322
 ?323
 ?324
 ?325
 ?326
 ?327
 ?328
 ?329
 ?330
 ?331
 ?332
 ?333
 ?334
 ?335
 ?336
 ?337
 ?338
 ?339
 ?340
 ?341
 ?342
 ?343
 ?344
 ?345
 ?346
 ?347
 ?348
 ?349
 ?350
 ?351
 ?352
 ?353
 ?354
 ?355
 ?356
 ?357
 ?358
 ?359
 ?360
 ?361
 ?362
 ?363
 ?364
 ?365
 ?366
 ?367
 ?368
 ?369
 ?370
 ?371
 ?372
 ?373
 ?374
 ?375
 ?376
 ?377
 ?378
 ?379
 ?380
 ?381
 ?382
 ?383
 ?384
 ?385
 ?386
 ?387
 ?388
 ?389
 ?390
 ?391
 ?392
 ?393
 ?394
 ?395
 ?396
 ?397
 ?398
 ?399
 ?400
 ?401
 ?402
 ?403
 ?404
 ?405
 ?406
 ?407
 ?408
 ?409
 ?410
 ?411
 ?412
 ?413
 ?414
 ?415
 ?416
 ?417
 ?418
 ?419
 ?420
 ?421
 ?422
 ?423
 ?424
 ?425
 ?426
 ?427
 ?428
 ?429
 ?430
 ?431
 ?432
 ?433
 ?434
 ?435
 ?436
 ?437
 ?438
 ?439
 ?440
 ?441
 ?442
 ?443
 ?444
 ?445
 ?446
 ?447
 ?448
 ?449
 ?450
 ?451
 ?452
 ?453
 ?454
 ?455
 ?456
 ?457
 ?458
 ?459
 ?460
 ?461
 ?462
 ?463
 ?464
 ?465
 ?466
 ?467
 ?468
 ?469
 ?470
 ?471
 ?472
 ?473
 ?474
 ?475
 ?476
 ?477
 ?478
 ?479
 ?480
 ?481
 ?482
 ?483
 ?484
 ?485
 ?486
 ?487
 ?488
 ?489
 ?490
 ?491
 ?492
 ?493
 ?494
 ?495
 ?496
 ?497
 ?498
 ?499
 ?500

2197	FC	Fuego de Colima	quad4-tri3	372	384
2198	VD	Volcanic Deposits	quad4-tri3	245	273
2199	GF	Graben Fill	quad4-tri3	456	338
2200	B	Basament	quad4-tri3	3088	2907
2201	CG	Colima graben	quad4-tri3	48	71
2202	Total Elements: 4209				

2203 **Table 2** - Rock mass and mechanical properties of the geological Units used in the finite-element
2204 model (from Norini et al., 2010, 2019).

2205

Acronym	Model Unit	Rock Type	Density (kg/m ³)	Young's Modulus (MPa)	Poisson's ratio ν
FC	Fuego de Colima	Andesitic lavas and pyroclastic deposits forming the Paleofuego-Fuego de Colima volcano	2242	1.4×10^3	0.30
VD	Volcaniclastic deposits	Pyroclastic and epiclastic deposits covering the southern flank of the CVC	1539	1.7×10^3	0.32
GF	Graben Fill	Quaternary alluvial, colluvial, lacustrine deposits filling the graben	1834	1.5×10^3	0.35
B	Basement	Cretaceous limestones and intrusive rocks forming the bed-rock underlying the CVC	2650	3.6×10^4	0.30

2206

2207

2208 Figures Captions

2209

2210 **Fig. 1** (a) Morphotectonic map of the Colima Volcanic Complex (NC=Nevado de Colima volcano;
2211 FC=Fuego de Colima volcano) and Colima Rift with the main tectonic and volcano-tectonic
2212 structures (NCG =Northern Colima Graben; CCG= Central Colima Graben, from Norini et al., 2019).
2213 In the inset, the location of the Colima Volcanic Complex (CVC) within the Trans-Mexican Volcanic
2214 Belt (TMVB) is shown in the frame of the subduction-type geodynamic setting of Central America
2215 (from Davila et al., 2019); (b) general sketch of the geometrical configurations used in LISA; (c)
2216 example of mesh of the investigated area for the dual magma chamber model with conduits (case v in
2217 panel (b), considering zero-displacement along the bottom and left and right sides. Note that for case

!218 (vi) in panel (b) the zero-displacement is removed from the lateral sides; (d) sketch of the Fuego de
!219 Colima feeding system composed of a 15 km-deep magma chamber connected to surface via a 6 km-
!220 deep magma chamber and dykes. ΔP_{chs} and ΔP_{chd} indicate either excess or over pressure
!221 (depending on the model used) in the shallow and deep chambers, respectively (modified from
!222 Massaro et al., 2019).

!223

!224 **Fig. 2** Results of the sensitivity analysis carried out on the Young Modulus variations within each
!225 rock layer of the domain considering different configurations (stratified substratum model – nodes:
!226 4426; single magma chamber model – nodes: 4426; dual magma chamber model – nodes: 4161; dual
!227 magma chamber with conduits model – nodes: 3737). For each geological Unit (B, FC, GF, VD), the
!228 relative global variation in L_2 (%) is provided for σ_1 and σ_3 . The $x(-)$ and $x(+)$ vectors indicate the
!229 Young's Modulus variation by an order of magnitude with respect to x_{ref} vector, containing the stress
!230 values calculated by using the values of material's properties indicated in Table 2.

!231

!232 **Fig. 3** Spatial variation (%) of the L_2 norm's components at varying Young Modulus for selected
!233 cases of Units B and VD: (a) Unit B in the stratified substratum model (nodes: 4426); (b) Unit B in
!234 the single magma chamber model (nodes: 4426); (c) Unit B in the dual magma chamber model
!235 (nodes: 4161); (d) Unit VD in the dual magma chamber with conduits model (nodes: 3737). Symbols
!236 $x(-)$ and $x(+)$ have the same meaning of Figure 2.

!237

!238 **Fig. 4** E-W gravitational modelling of the CVC domain. The scale of the mesh is expressed in Unit
!239 of Design (1 UD = 1 km). The domain extends 60 km along the x -axis, and 30 km along the z -axis.
!240 The number of nodes used in the mesh is set to 4426. The magnitude and pattern of the principal
!241 stresses (dotted black lines) are reported for (a) the homogeneous stratigraphy (Unit FC =andesitic
!242 lavas and pyroclastic deposits) and for (b) the not homogeneous stratigraphy (Unit FC; Unit B=
!243 Cretaceous limestones and intrusive rocks forming the bed-rock underlying the CVC; Unit GF=
!244 Quaternary alluvial, colluvial, and lacustrine deposits filling the graben; Unit VD= volcanoclastic
!245 deposits covering the southern flank of the CVC). The blue line contours the unperturbed part of the
!246 domain, which extends ca. 30 km horizontally and ca. 25 km vertically. Note that the scale of stress
!247 values is the same for the all simulations.

!248

!249

!250 **Fig. 5** E-W gravitational modelling of the CVC domain with a not homogeneous stratigraphy. The
!251 magnitude and pattern of the principal stresses are reported for (a) the single magma chamber model
!252 represented by a magma chamber ($2a = 14$ km and $2b = 3.6$ km) at 15 km of depth, and (b) the dual
!253 magma chamber model composed of a 15 km-deep magma chamber ($2a = 14$ km and $2b = 3.6$ km)

Utente di Microsoft Office 25/9/20 12:16
Eliminato: 's

Silvia 25/9/20 14:37
Eliminato: 's

Silvia 25/9/20 14:37
Eliminato: 's

‡257 and a shallow 6 km-deep one ($2a = 3.5$ km and $2b = 2$ km). The magma chambers are not connected.
‡258 ΔP_o is set to 10 and 5 MPa for the 15 km-deep and 6 km-deep magma chambers, respectively. The
‡259 number of nodes is set to 4426 and 4161 for the single and dual magma chamber models, respectively.
‡260 Black dotted lines highlight the passage from different stress values. The red dotted line in panel (b-i)
‡261 indicates the formation of the stress arch. Note that the scale of stress values are different for each
‡262 panel in order to maximise the simulation details.

‡263

‡264 **Fig. 6** E-W gravitational modelling of the CVC domain with a not homogeneous stratigraphy
‡265 accounted for a dual magma chamber system connected by dykes via surface (deep magma chamber,
‡266 $2a = 14$ km and $2b = 3.6$ km at 15 km of depth; shallow magma chamber, $2a = 3.5$ km and $2b = 2$ km
‡267 at 6 km of depth). The magnitude and pattern of the principal stresses are shown. The number of
‡268 nodes used is set to 3737. ΔP_o is set to 10 and 5 MPa for the 15 km-deep and 6 km-deep magma
‡269 chambers, respectively. The black dotted lines in panel (ii) highlight the passage from different stress
‡270 values. Note that the scale of stress values are different for each panel in order to maximise the
‡271 simulation details.

‡272

‡273 **Fig. 7** E-W gravitational modelling of the CVC domain with a not homogeneous stratigraphy
‡274 considering the extensional field stress. The magnitude and pattern of the principal stresses are shown
‡275 for the single magma chamber model (panels i-ii), the dual magma chamber model (panels iii-iv), the
‡276 dual magma chamber with conduits model (panels v-vi-vii-viii). Note that in panel vii-viii the faults
‡277 bordering the CG are shown. For all configurations an extensive far-field stress of 5 MPa is applied at
‡278 the lateral boundaries of the domain. In panels vii-viii the additional effect of the local extensive field
‡279 is simulated using a reduced values of material's properties (Table 2). ΔP_o is set to 10 and 5 MPa for
‡280 the 15 km-deep and 6 km-deep magma chambers, respectively. Black dotted lines highlight the
‡281 passage from different stress values. The red arrows indicate the direction of the applied far field
‡282 stress. Note that the scale of stress values are different for each panel in order to maximise the
‡283 simulation details.

‡284

‡285

‡286

‡287

‡288

Silvia 20/9/20 11:13
Eliminato: The magmatic overpressures are
Silvia 25/9/20 14:36
Formattato: Tipo di carattere:10 pt

Silvia 20/9/20 11:14
Eliminato: The magmatic overpressures are
Silvia 25/9/20 14:36
Formattato: Tipo di carattere:9 pt

Silvia 20/9/20 11:15
Eliminato: Colima graben

Silvia 25/9/20 14:36
Formattato: Tipo di carattere:10 pt
Silvia 20/9/20 11:15
Eliminato: The magmatic overpressures are

293

294

295

296 **Figures**

297

298

299

300

301

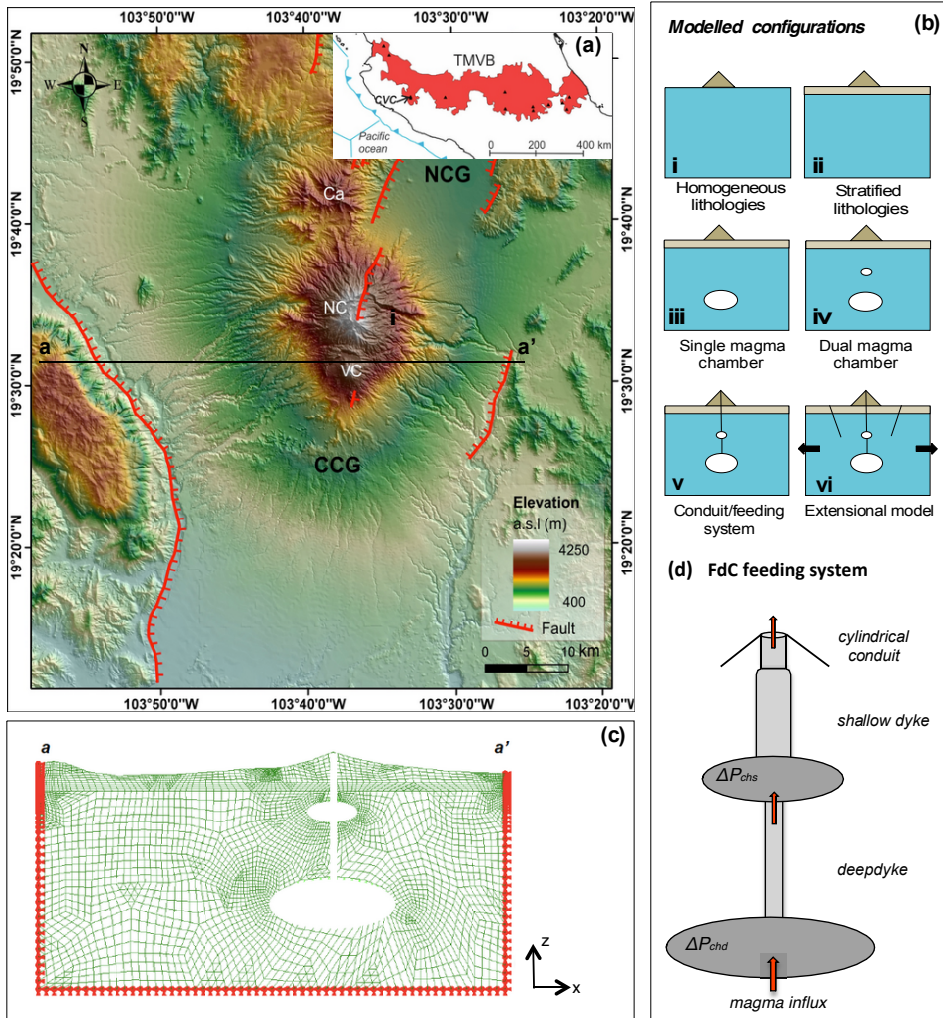
302

303

304

305

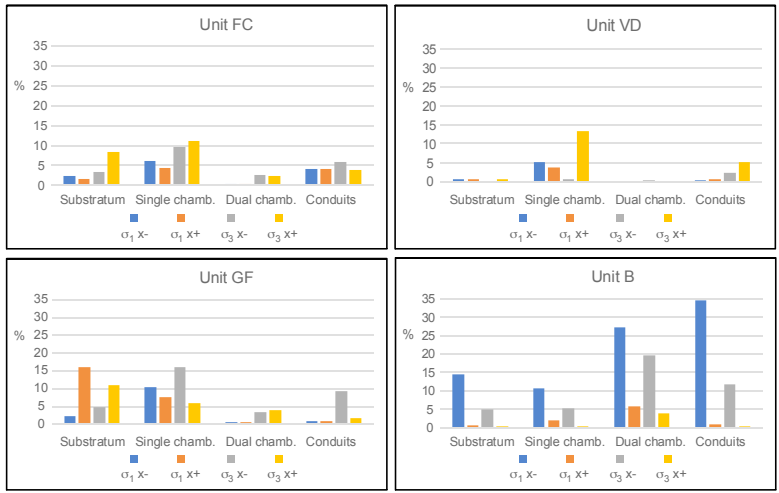
306 **Figure 1**



307

308

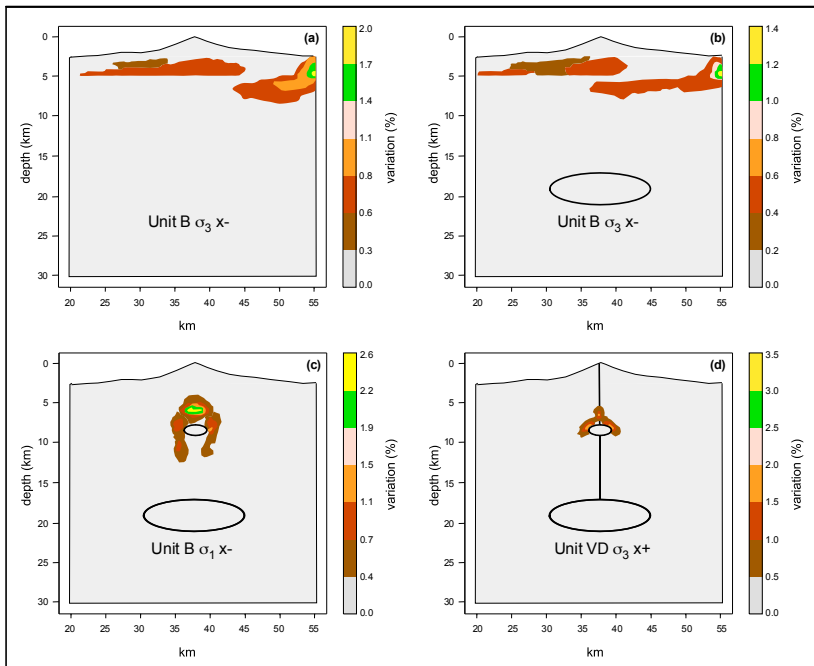
309 Figure 2



310

311

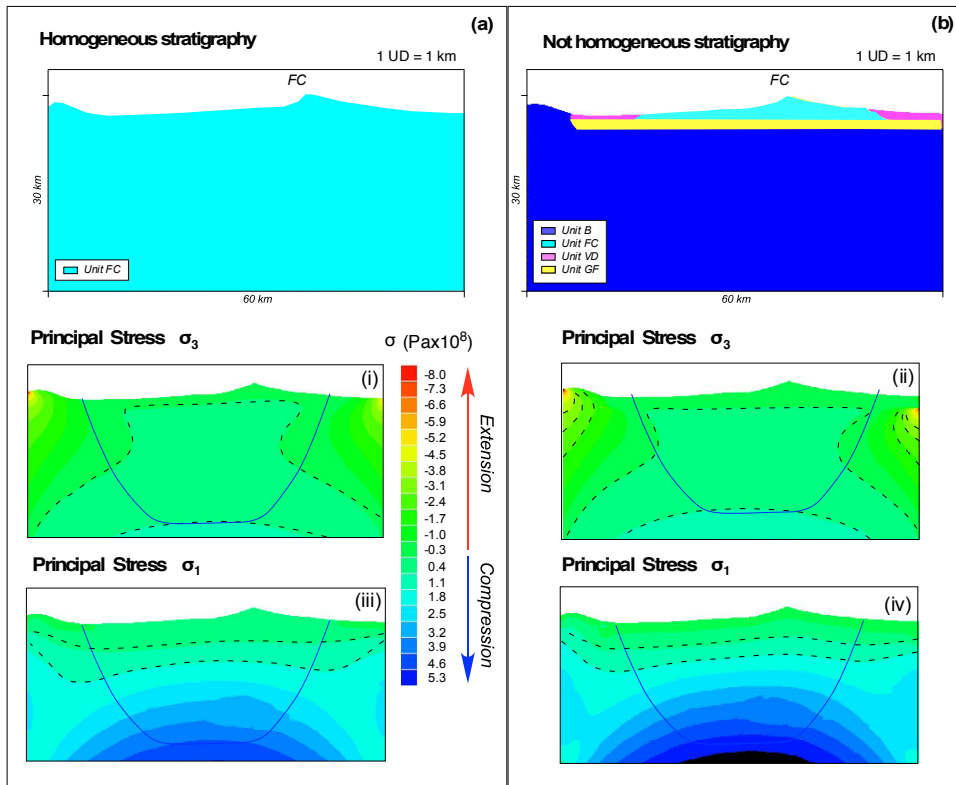
312 Figure 3



313

314

315 Figure 4



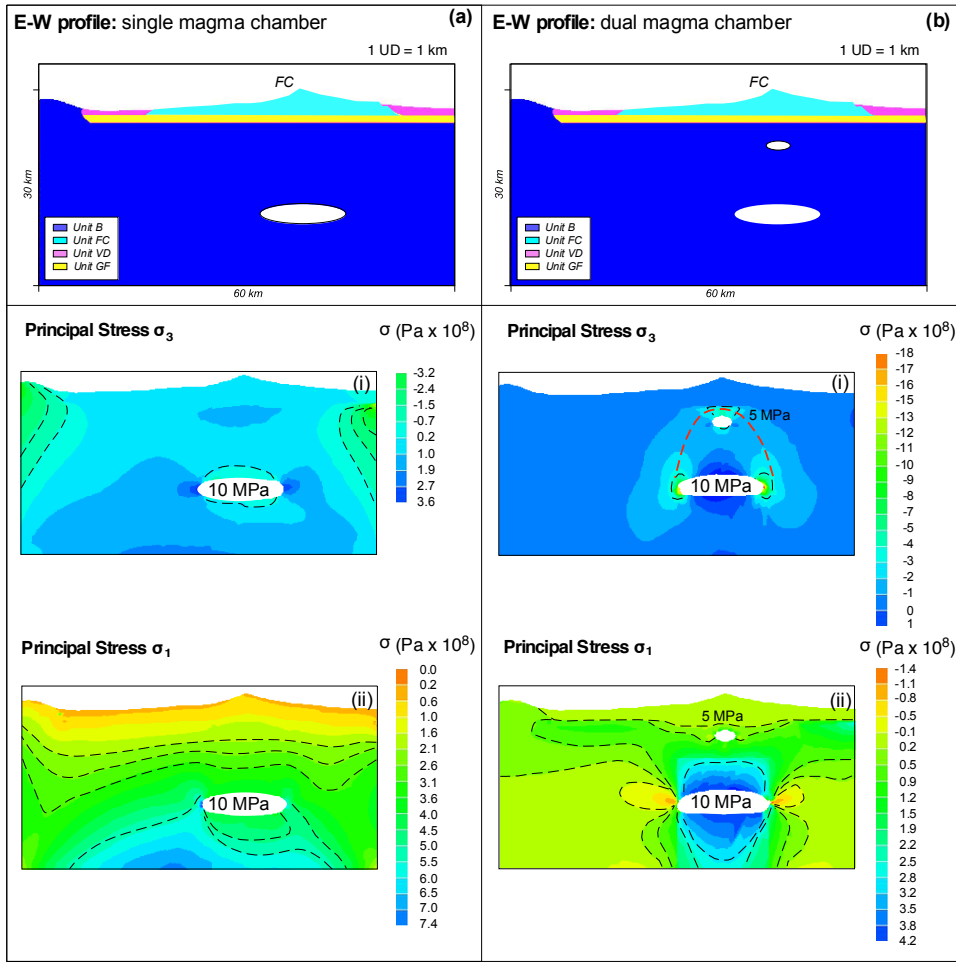
316

317

318

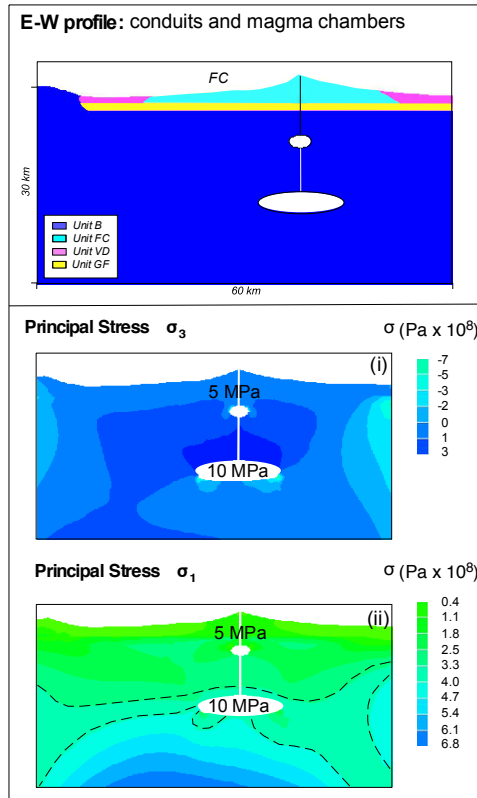
319

320 Figure 5



321
322
323
324
325

Figure 6



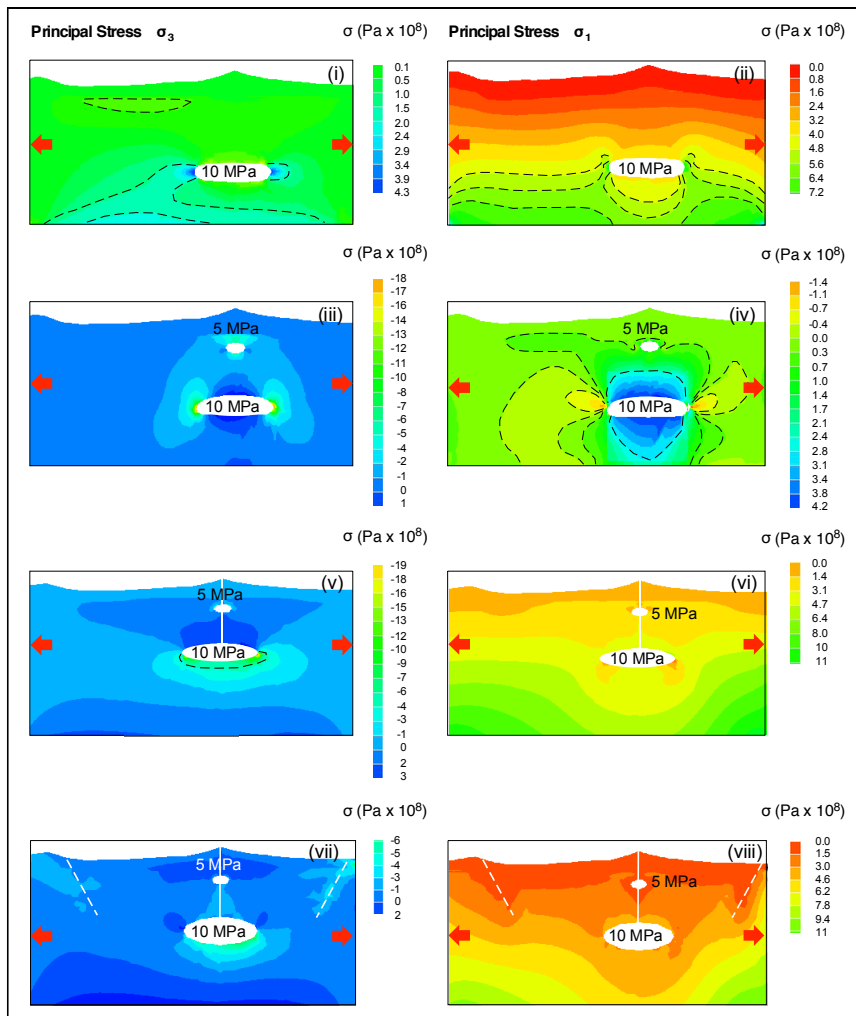
1326

1327

1328

1329

1330 Figure 7

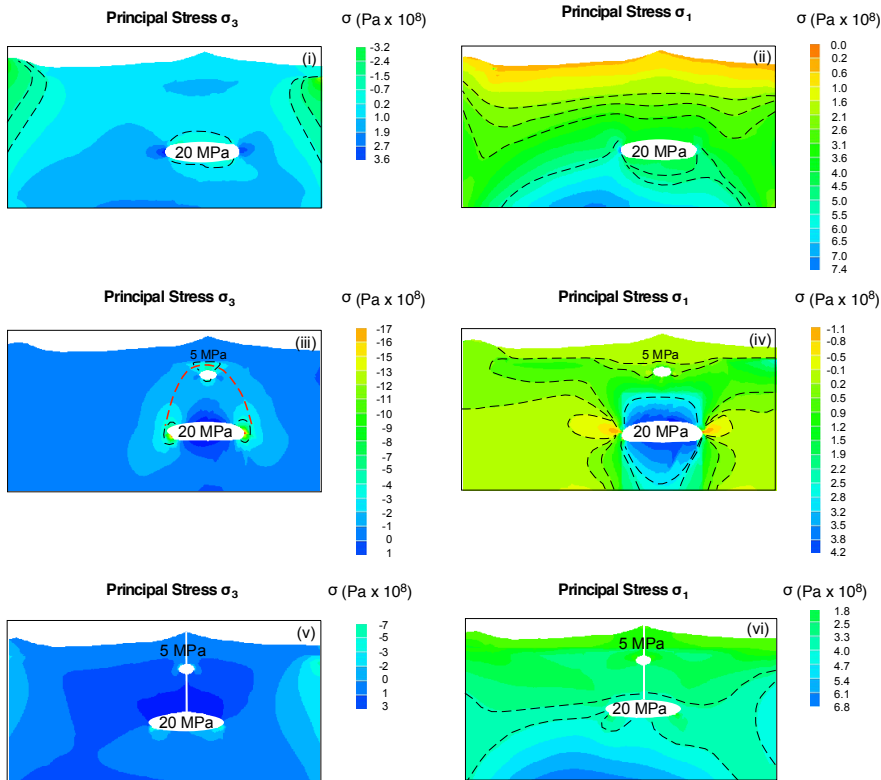


331

332

333 Appendix 1

Appendix 1



!334

!335

!336 Appendix 2

Appendix 2

